

NASA CR-165585
ODAL-1403-12-81

(NASA-CR-165585) DEVELOPMENT OF A
SIMPLIFIED PROCEDURE FOR THRUST CHAMBER LIFE
PREDICTION Final Report (O'Donnell and
Associates, Inc.) 85 p HC A05/MF A01

N82-21253

Unclas

CSCCL 21H 63/20 09497

Development of a Simplified Procedure For Thrust Chamber Life Prediction

by

J. S. Porowski
M. Badlani
B. Kasraie
W. J. O'Donnell
D. Peterson

O'DONNELL & ASSOCIATES,
241 Curry Hollow Road
Pittsburgh, Pennsylvania 15201



Prepared for

NATIONAL AERONAUTICS AND SPACE ADMINISTRATION
Lewis Research Center
Cleveland, Ohio 44135
Contract NAS3-22649

1. Report No.	2. Government Accession No.	3. Recipient's Catalog No. NASA CR-165585	
4. Title and Subtitle Development of a Simplified Procedure for Thrust Chamber Life Prediction		5. Report Date October 1981	6. Performing Organization Code
		8. Performing Organization Report No. ODAI-1403-12-81	
7. Author(s) J. S. Porowski, M. Badlani, B. Kasraie, W. J. O'Donnell, D. Peterson		10. Work Unit No.	11. Contract or Grant No. NAS3-22649
9. Performing Organization Name and Address O'Donnell & Associates, Inc. 241 Curry Hollow Road Pittsburgh, Pennsylvania 15236		13. Type of Report and Period Covered Final Report	
		14. Sponsoring Agency Code	
12. Sponsoring Agency Name and Address National Aeronautics & Space Administration Lewis Research Center Cleveland, Ohio 44135		15. Supplementary Notes H. J. Kasper, NASA Technical Monitor	
16. Abstract <p>An analytical design procedure for predicting thrust chamber life considering cyclically induced thinning and bulging of the hot-gas-wall is developed. The hot-gas-wall, composed of ligaments connecting adjacent cooling channel ribs and separating the coolant flow from the combustion gas, is subjected to pressure loading and severe thermal cycling. Thermal transients during start-up and shut-down cause plastic straining through the ligaments. The primary bending stress superimposed on the alternate in-plane cyclic straining causes incremental bulging of the ligaments during each firing cycle. This basic mechanism of plastic ratcheting is analyzed and a method developed for determining ligament deformation and strain. The method uses a yield surface for combined bending and membrane loading to determine the incremental permanent deflection and progressive thinning near the center of the ligaments which cause the geometry of the ligaments to change as the incremental strains accumulate. Fatigue and tensile instability are affected by these local geometry changes. Both are analyzed and a failure criterion developed. Results of the simplified analyses are shown to compare favorably with experimental data and finite element analysis results for OFHC (Oxygen Free High Conductivity) copper. They are also in reasonably good agreement with experimental data for NARloy Z, a copper-zirconium-silver alloy developed by the Rocketdyne Division of Rockwell International.</p>			
17. Key Words (Suggested by Author(s)) Rocket engines, nozzles, thrust chambers, structural fatigue, stress analysis		18. Distribution Statement Unclassified - Limited	
19. Security Classif. (of this report) Unclassified	20. Security Classif. (of this page) Unclassified	21. No. of Pages 87	22. Price*

* For sale by the National Technical Information Service, Springfield, Virginia 22161

PRECEDING PAGE BLANK NOT FILMED

DEVELOPMENT OF A SIMPLIFIED PROCEDURE
FOR THRUST CHAMBER LIFE PREDICTION

Table of Contents

	<u>Page</u>
SUMMARY	1
1.0 INTRODUCTION	2
2.0 PLUG NOZZLE THRUST CHAMBER	3
3.0 DEVELOPMENT OF A SIMPLIFIED ANALYTICAL MODEL FOR CALCULATING HOT-GAS-WALL DEFORMATION AND STRAIN	5
3.1 Simplified Model	5
3.2 Analysis of Basic Mechanism of Plastic Ratcheting	7
3.3 Interaction of Shear Stress	12
3.4 Deformation History	15
3.5 Stress and Strain Resultants	18
3.6 Thermally Induced Stresses	23
4.0 DEVELOPMENT OF FAILURE MODE EVALUATION CRITERION	27
4.1 Plastic Instability - Necking	27
4.2 Strain Range - Fatigue	32
5.0 THRUST CHAMBER LIFE PREDICTIONS	35
6.0 FINITE ELEMENT ANALYSIS	37
7.0 COMPARISON OF RESULTS	38
8.0 CONCLUSIONS	38
9.0 REFERENCES	40
APPENDIX A Numerical Examples	41
APPENDIX B Finite Element Analysis	60
APPENDIX C Fortran Program for Fatigue Calculations	78
APPENDIX D Symbols	80

DEVELOPMENT OF A SIMPLIFIED PROCEDURE
FOR THRUST CHAMBER LIFE PREDICTION

SUMMARY

An analytical design procedure for predicting thrust chamber life considering cyclically induced thinning and bulging of the hot-gas-wall is developed. The hot-gas-wall, composed of ligaments connecting adjacent cooling channel ribs and separating the coolant flow from the combustion gas, is subjected to pressure loading and severe thermal cycling. Thermal transients during start-up and shut-down cause plastic straining through the ligaments. The primary bending stress superimposed on the alternate in-plane cyclic straining causes incremental bulging of the ligaments during each firing cycle. This basic mechanism of plastic ratcheting is analyzed and a method developed for determining ligament deformation and strain. The method uses a yield surface for combined bending and membrane loading to determine the incremental permanent deflection and progressive thinning near the center of the ligaments which cause the geometry of the ligaments to change as the incremental strains accumulate. Fatigue and tensile instability are affected by these local geometry changes. Both are analyzed and a failure criterion developed. Results of the simplified analyses are shown to compare favorably with experimental data and finite element analysis results for OFHC (Oxygen Free High Conductivity) copper. They are also in reasonably good agreement with experimental data for NARloy Z, a copper-zirconium-silver alloy developed by the Rocketdyne Division of Rockwell International.

DEVELOPMENT OF A SIMPLIFIED PROCEDURE
FOR THRUST CHAMBER LIFE PREDICTION

1.0 INTRODUCTION

Life predictions of regeneratively liquid cooled rocket thrust chambers have been based on low cycle fatigue principles. Tests of thrust chambers, however, [1, 2]* revealed that coolant channel walls in the failed areas have exhibited progressive incremental thinning and bulging during the heating and cooling cycle associated with each firing. Failure analyses performed as a part of this work indicate that ductile rupture is a more limiting mode of failure than fatigue failure. Thus, material tensile instability was considered in addition to fatigue damage mechanisms in the present structural evaluation.

The mechanism of hot-gas-wall or ligament incremental distortion can be investigated by inelastic finite element analyses. For the cyclic histories of interest, however, such analyses are difficult to perform and require extensive computer time. Their use for a single characteristic case is feasible and provides valuable information. In fact, such analyses were carried out within NASA-Lewis research programs for simplified histories of thermal loading. Such methods, however, are not suitable for evaluating the effects of changing various design and operating parameters such as geometric configurations, material properties, pressures and temperatures. More general methods which do not require lengthy inelastic finite element solutions are therefore needed.

The present work is aimed at: (1) analyzing the failure mode of the cyclically loaded thrust chamber, (2) developing simplified but conservative methods for evaluating the strains

*Numbers in brackets designate references at end of report.

and deformations, and (3) providing methods for predicting the cyclic life of the thrust chamber.

One or two cycles of elastic and inelastic analysis were analyzed to determine stress and strain resultants for the simplified models. Other available inelastic finite element results and test data were also used to determine the accuracy of the simplified models.

The scope of the work is as follows:

1. Develop a simplified analytical model for determining hot-gas-wall deformation and strain.
2. Determine accuracy of simplified model by comparison with inelastic finite element analysis results.
3. Develop a failure mode evaluation criterion.
4. Provide a simple design procedure for making life predictions for thrust chambers.

Each of these items will be discussed in the sections to follow. Also the assumptions made in the development of the analysis procedure for each item are discussed in their respective sections.

2.0 PLUG NOZZLE THRUST CHAMBER

The plug nozzle thrust chamber shown in Figure 1 is considered. Figure 1 provides dimensions for the thrust chamber tested at NASA Lewis Research Center. The sample solution and computer finite element calculations given in the Appendices were performed for this thrust chamber. However, the resulting simplified method of analysis is applicable for a general case where the geometry, loading conditions and materials can be altered to comply with the design of a specific engine. The

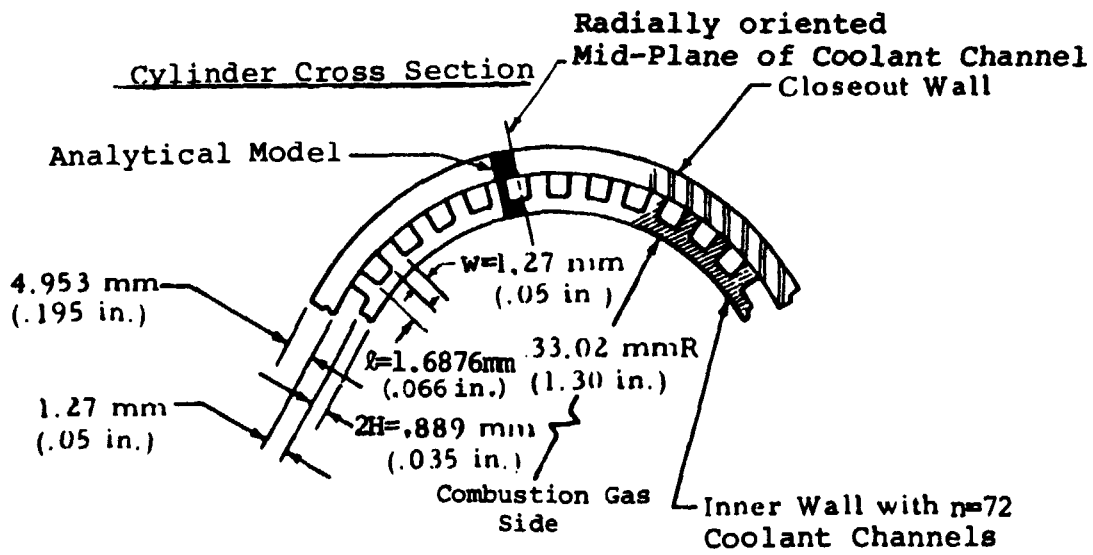
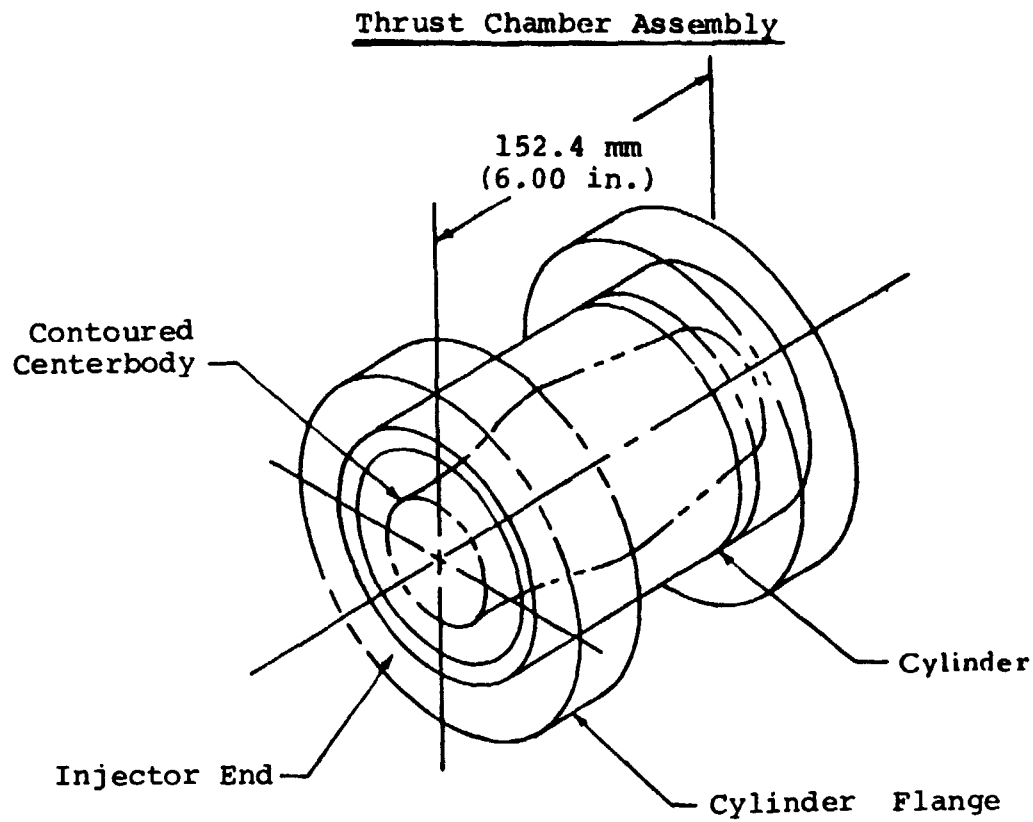


FIGURE 1 PLUG NOZZLE THRUST CHAMBER

plug nozzle assembly consisting of the contoured centerbody and flanged cylinder is shown along with cross sectional details of the cylinder. The inner liner of the cylinder contains axial flow coolant channels of constant cross section and is constructed from either OFHC copper, half-hard Amzirc (American Metal Climax, Inc. copper alloy) or NARloy-Z. The closeout wall is electroformed copper in all cases. Since no failures occurred in the centerbody only the cylindrical part of the nozzle was investigated.

Typical firing cycle history data for the thrust chamber is illustrated in Figure 2. The data refer to the critical section where failures were observed during testing. Only this section was considered in the analysis. The first cycle begins with a cooling period when the liquid hydrogen enters the channels. The uniform temperature 29°K (53°R) is reached before a sudden rise of temperature beginning at the ignition point of 1.5 seconds.

The mechanical properties used to characterize the cylinder wall materials were provided by NASA-Lewis. Reference 3 provides temperature dependent thermal expansion, modulus of elasticity and static stress-strain properties of half-hard Amzirc, NARloy-Z, annealed OFHC and EFCU (electroformed copper).

3.0 DEVELOPMENT OF A SIMPLIFIED ANALYTICAL MODEL FOR CALCULATING HOT-GAS-WALL DEFORMATION AND STRAIN

3.1 Simplified Model

The inner wall shown in Figure 1 separating the coolant flow and the combustion gas is subjected to severe thermal cycling. The temperature difference between the closeout and inner walls that occurs during the thermal transient causes plastic straining through the ligament within the

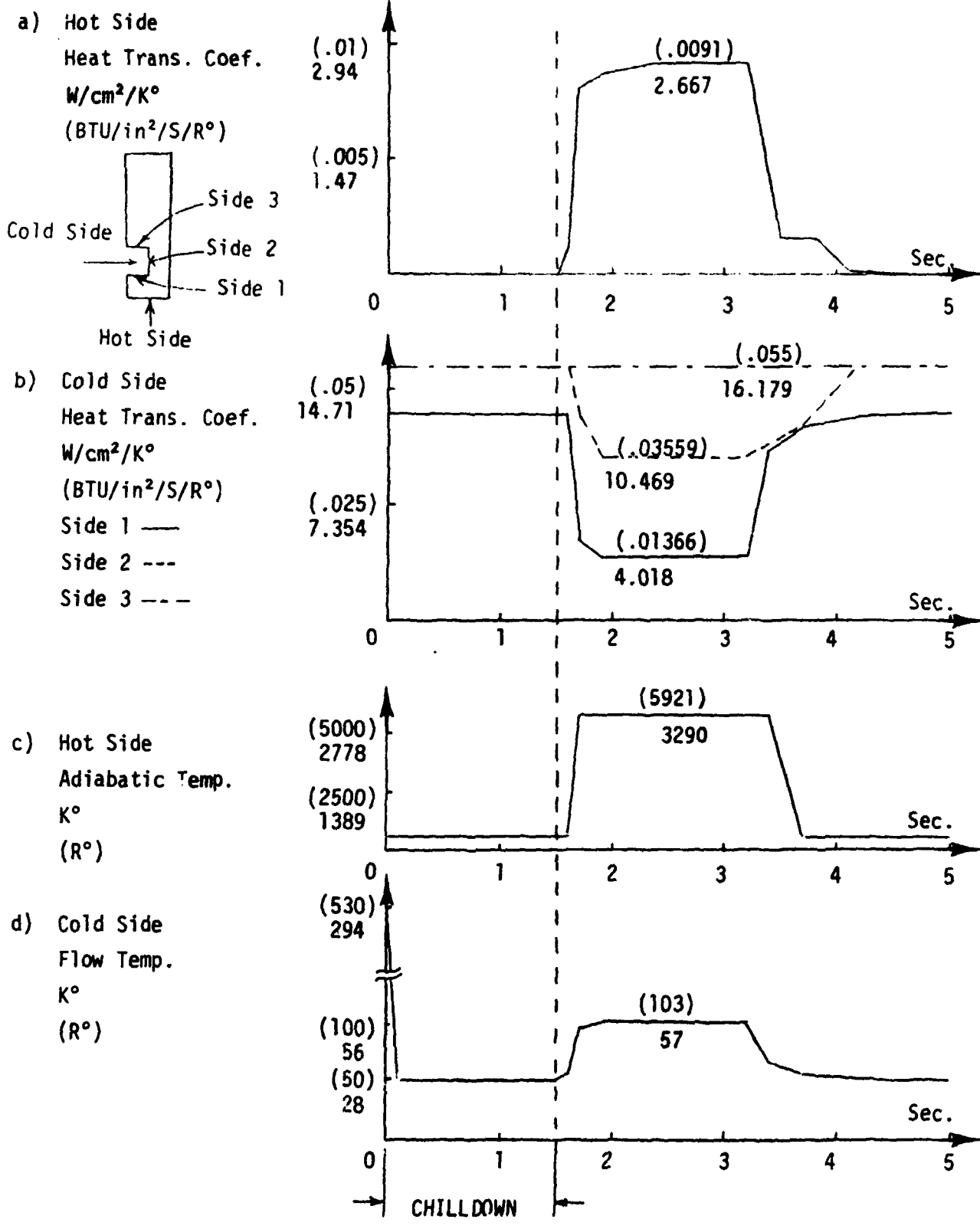


FIGURE 2 THE TIME HISTORIES OF HEAT TRANSFER COEFFICIENTS AND TEMPERATURES FOR A CHILLDOWN AND FIRING CYCLE

range of 1 to 2 percent. The temperature history for the closeout and inner walls at the middle plane of the cooling channel is shown for one cycle in Figure 3. The inner wall is attached to the closeout wall by radial ribs. The outer wall remains elastic within the entire thermal cycle forcing the inner wall ligaments into captive plastic straining. Straining in the hoop direction is accompanied by high axial strains.

The ligaments separating the coolant and the combustion gas are subjected to coolant pressure load and thermally induced through-the-wall bending. The resulting stresses interact during plastic straining causing incremental bulging or ratcheting directed radially inward. The mechanism of pressure induced ratcheting is illustrated in Figure 4. Primary bending stresses persist during alternate in-plane cyclic straining resulting in a small repetitive incremental permanent deflection of the ligaments during each firing cycle. The simple model in Figure 4 does not include interaction of shear stress due to pressure and the thermally induced bending. Their effects are evaluated later in the report.

3.2 Analysis of Basic Mechanism of Plastic Ratcheting

The approach used to determine increments of plastic strain within the load cycles is explained in Figure 5. The axial forces and bending moments acting on the rectangular cross section as shown in Figure 5a are considered. The bar simulates the response of the ligament of a cooling channel between the two ribs. The bar is cyclically stretched and squeezed plastically in the presence of sustained bending. Note that the "X" direction in the beam model corresponds to the hoop direction in the ligament.

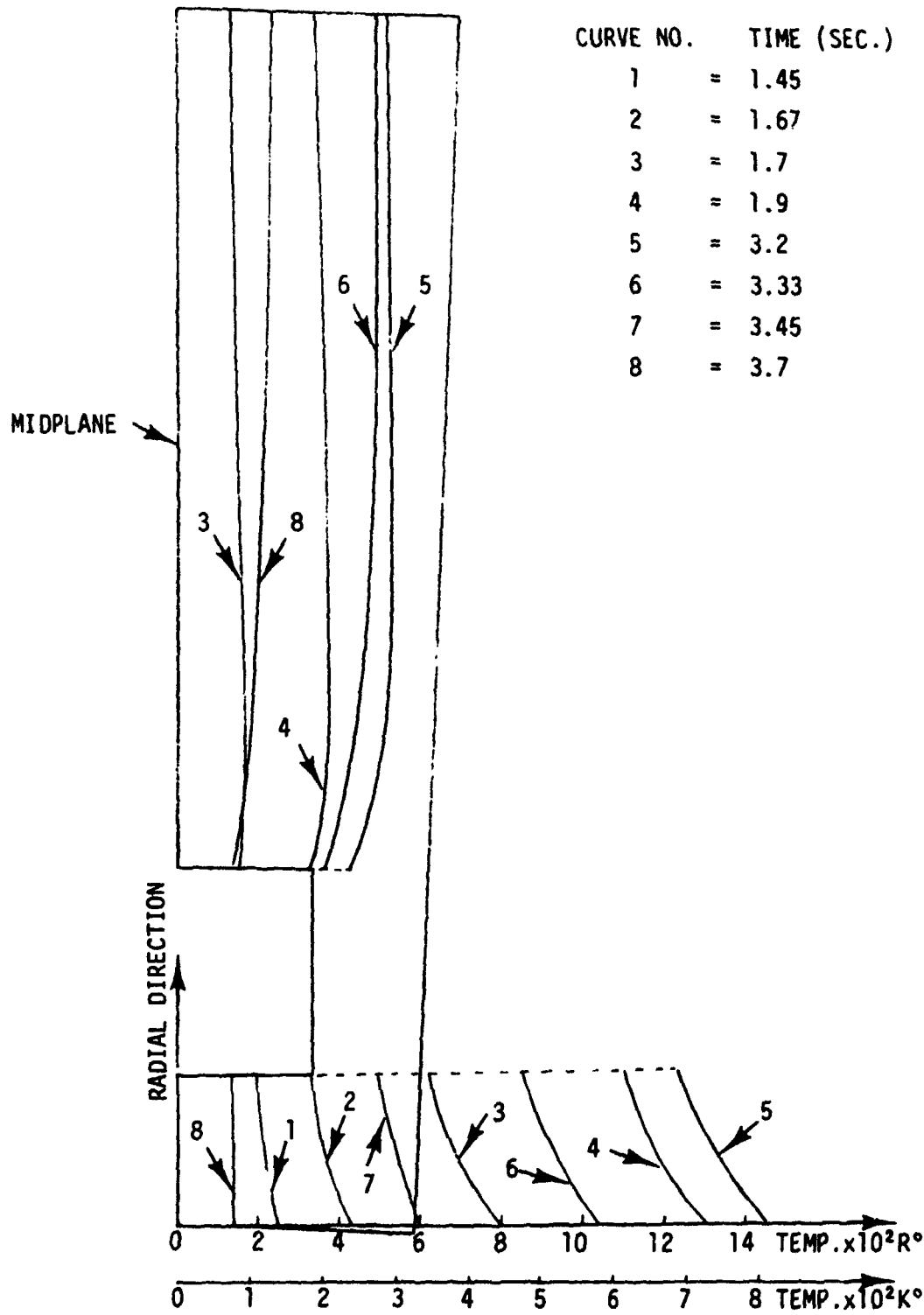


FIGURE 3 MIDPLANE TEMPERATURE HISTORY

CLOSE-OUT WALL

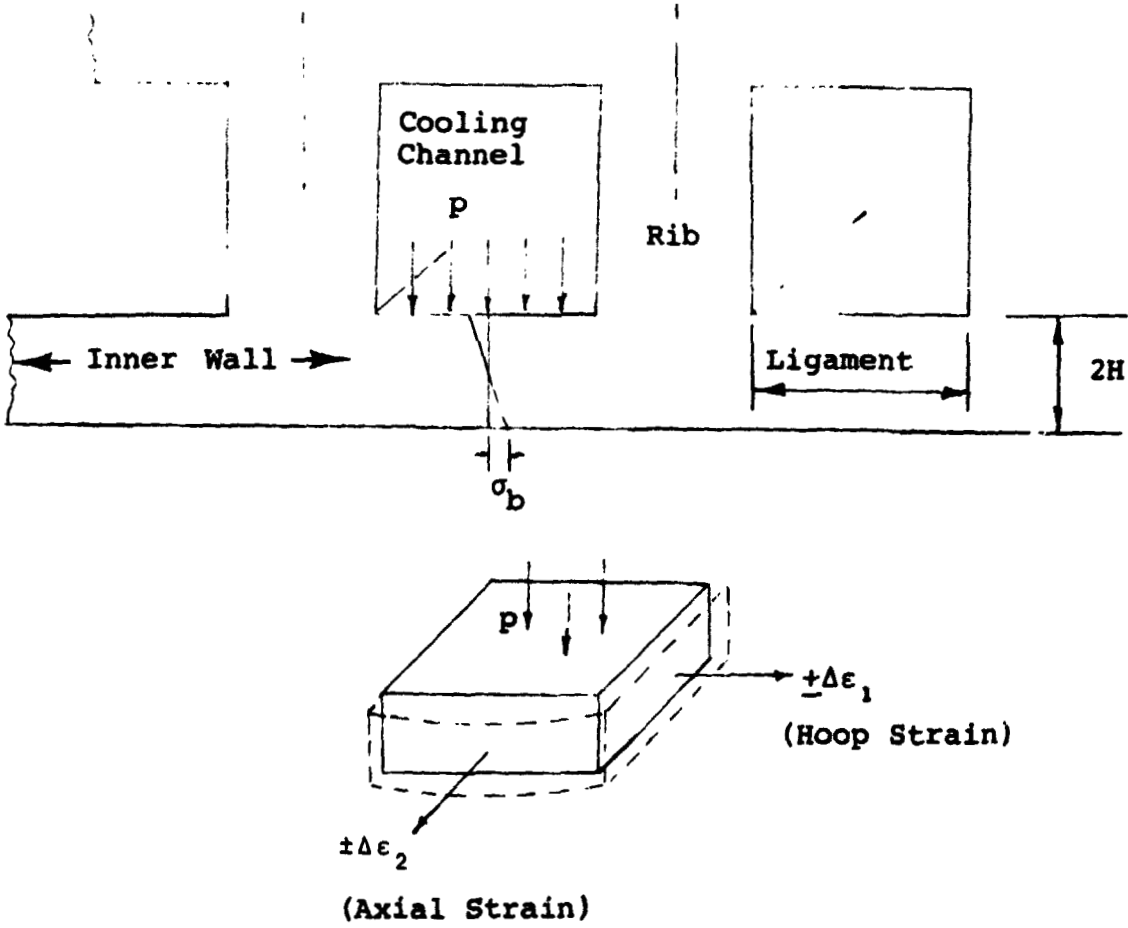
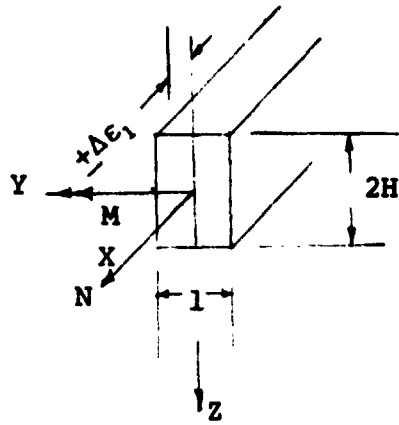


FIGURE 4 ELASTIC RATCHETING DUE TO INTERACTION OF PRESSURE AND THERMAL CYCLING

a)



X - Hoop Direction
Y - Axial Direction

b)

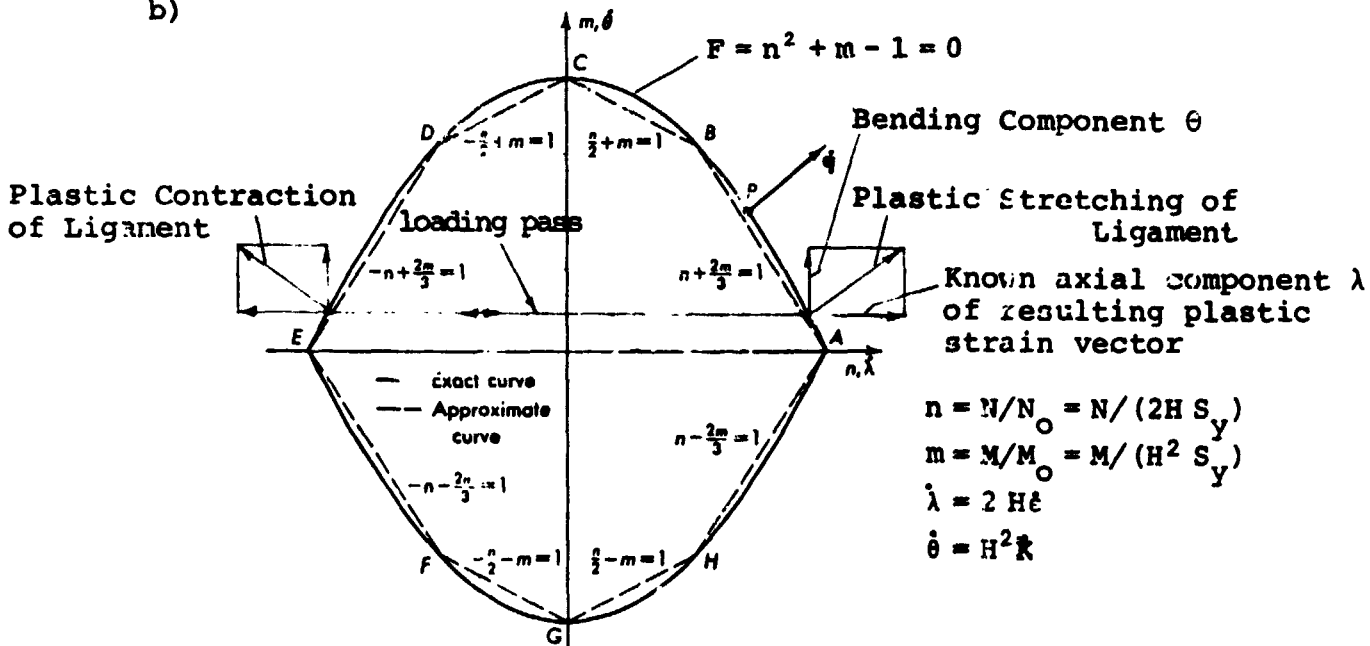


FIGURE 5 PLASTIC RATCHET INCREMENTS IN A BAR OF RECTANGULAR CROSS SECTION SUBJECTED TO SUSTAINED BENDING MOMENT AND CYCLIC AXIAL STRAIN

- a) Ligament Beam Element Loading
b) Interaction Curve

To obtain a conservative bound on the plastic strain increments, strain hardening of the material is ignored.

The yield curve for a beam subjected to bending and axial force is composed of two parabolas as shown in Figure 5b and is defined by the relation, [4]:

$$F = m + n^2 - 1 = 0 \quad (1)$$

where m and n are dimensionless variables defined by:

$$m = \frac{M}{M_0} \quad (2a)$$

$$n = \frac{N}{N_0} \quad (2b)$$

In the above, M and N denote the bending moment and axial force, while M_0 and N_0 denote the yield bending moment and yield axial force given by:

$$M_0 = H^2 S_y \quad (3a)$$

$$N_0 = 2H S_y \quad (3b)$$

for a rectangular beam of unit width, height $2H$ and yield stress S_y .

Plastic flow vectors \dot{q} are normal to the yield curve. The curve is plotted using generalized stresses n and m related to axial and bending tractions, respectively. The associated generalized strain rates $\dot{\lambda}$ and $\dot{\theta}$ are defined by the average hoop strain rate $\dot{\epsilon}$ and the rate of curvature of the bent bar, \dot{K} , respectively, as shown in Figure 5. If hoop increments of plastic strain are known the corresponding increment of curvature is defined by the slope of the yield surface and can be determined (based on the normality

of resulting strain rate vector \dot{q}) as shown in Figure 5b.

The generalized strain rates can be obtained by partial differentiation of equation (1) as follows:

$$\dot{\lambda} = A \frac{\partial F}{\partial n} = 2nA \quad (4a)$$

$$\dot{\theta} = A \frac{\partial F}{\partial m} = A \quad (4b)$$

where A is an arbitrary positive scalar. Thus, for the interaction of hoop and bending loads, the relation between $\dot{\lambda}$ and $\dot{\theta}$ components of the \dot{q} vector is simply:

$$\frac{\dot{\theta}}{\dot{\lambda}} = \left(\frac{\theta}{\lambda} \right) = \frac{1}{2n} \quad (5)$$

For known values of bending m which remain constant within the cycle, n can be obtained from the yield line of equation (1). Hoop increments of plastic strain are being reversed within two halves of the thermal cycle. However, plastic increments of curvature within each half of the thermal cycle are of the same sign. Thus, they accumulate causing incremental bulging of the cooling channel wall.

3.3 Interaction of Shear Stress

For high pressures in the cooling channels the model of the thrust chamber must also include shear stress τ . The method of solution is analogous. However, the solution includes generalized shear stress and the corresponding shear strain.

The yield surface based on Tresca's yield criterion is given by Peterson *et al.*

$$F = m + \frac{n^2}{k} - k = 0 \quad (6a)$$

where

$$k = \sqrt{1 - s^2} \quad (6b)$$

and $s = \frac{2\tau}{S_y}$ is the dimensionless shear stress.

The generalized strains λ , θ and ϕ are related to the hoop strain, curvature and shear strain, respectively. Using the normality law:

$$\dot{\lambda} = A \frac{\partial F}{\partial n} = 2An \quad (7a)$$

$$\dot{\theta} = A \frac{\partial F}{\partial m} = A \sqrt{1 - s^2} \quad (7b)$$

$$\dot{\phi} = A \frac{\partial F}{\partial s} = A \left(2s - \frac{ms}{\sqrt{1 - s^2}} \right) \quad (7c)$$

The proportions between the strain components are thus:

$$\frac{\partial F}{\partial m} : \frac{\partial F}{\partial n} : \frac{\partial F}{\partial s} = \left(\sqrt{1 - s^2} \right) : (2n) : \left(2s - \frac{ms}{\sqrt{1 - s^2}} \right) \quad (8)$$

The generalized variables λ , θ and ϕ can be related to the hoop strain, curvature and shear strain by considering the rate of dissipation D given by [4]:

$$D = M\dot{\kappa} + N\dot{\epsilon} + S\dot{\gamma} \quad (9)$$

where M , N and S denote the bending moment, hoop force and shear force, respectively, and $\dot{\kappa}$, $\dot{\epsilon}$ and $\dot{\gamma}$ denote the curvature rate, hoop strain rate and shear strain rate, respectively.

Using equation (2), equation (9) can be written as:

$$D = mM_o \dot{K} + nN_o \dot{\epsilon} + sS_o \dot{\gamma} \quad (10a)$$

where

$$s = \frac{S}{S_o} = \frac{2\tau}{S_y} = \frac{S}{H S_y} \quad (10b)$$

since the cross sectional area for unit width equals 2H.

Then using (3), (10a) and (10b):

$$D = S_y [m(H^2 \dot{K}) + n(2H \dot{\epsilon}) + s(H \dot{\gamma})] \quad (11a)$$

Also in terms of the generalized strain rates, the rate of dissipation is given by:

$$D = S_y [m \dot{\theta} + n \dot{\lambda} + s \dot{\phi}] \quad (11b)$$

Thus the relationship between the generalized strain rates and the hoop strain rate, curvature rate and shear strain rate are, respectively:

$$\dot{\lambda} = 2H \dot{\epsilon} \quad (12a)$$

$$\dot{\theta} = H^2 \dot{K} \quad (12b)$$

$$\dot{\phi} = H \dot{\gamma} \quad (12c)$$

For known increments of hoop strain λ and known values of m and s , the remaining components of strain θ and ϕ (shear) are determined by the ratios (8). Since the load point must remain on the yield surface, the known values of m and s determine n which is obtained from equation (6a).

The curvature and shear strain as determined from (12) can then be integrated along the length of the ligament to obtain the bending and shear deflections. Once the total deflection is known, the corresponding thinning in the ligament is calculated by assuming that the volume of the material remains constant. Integration of the deflection and determination of ligament thinning is described in Section 3.4.

It can be shown from the generalized yield surfaces derived in Ref. [5] that though the yield surface given by equation (6a) is derived for a uniaxial model, it also holds for biaxial conditions when $n_2 < n_1$ ($n_1 = n =$ hoop stress variable in equation (6a)) and m and s are small, as in the present case. Thus the generalized strain relationships derived above are also applicable for the biaxial case.

3.4 Deformation History

From equations (7a), (7b) and (12a), (12b):

$$\frac{\dot{\theta}}{\dot{\lambda}} = \frac{\theta}{\lambda} = \frac{\sqrt{1-s^2}}{2n} = \frac{H}{2} \frac{\dot{K}}{\dot{\epsilon}} = \frac{H}{2} \frac{K}{\epsilon} \quad (13)$$

For the complete cycle, the plastic strain generated by the temperature difference during heat-up in the hoop direction is fully reversed when the temperature becomes uniform at the end of the cycle. Thus,

$$\epsilon = \epsilon_1 = 2 \left(\Delta \epsilon_{p1} \right) \quad (14)$$

where $\Delta \epsilon_{p1}$ is given by sum of plastic strain range due to differential thermal expansion $\Delta \epsilon_{p1}^I$ and the correction due to thermally induced bending $\Delta \epsilon_{p1}^B$ which are evaluated in Sections 3.5 and 3.6, respectively.

Thus, the curvature is given by:

$$K = \frac{2\sqrt{1-s^2}}{n} \frac{(\Delta\epsilon_{p_1})}{H} \quad (15)$$

Similarly from equations (7a), (7c) and (12a), (12c):

$$\frac{\dot{\phi}}{\dot{\lambda}} = \frac{\phi}{\lambda} = \left(2s - \frac{ms}{\sqrt{1-s^2}} \right) / 2n = \dot{\gamma}/2\dot{\epsilon} = \gamma/2\epsilon \quad (16)$$

Making use of equation (14), the shear strain is then:

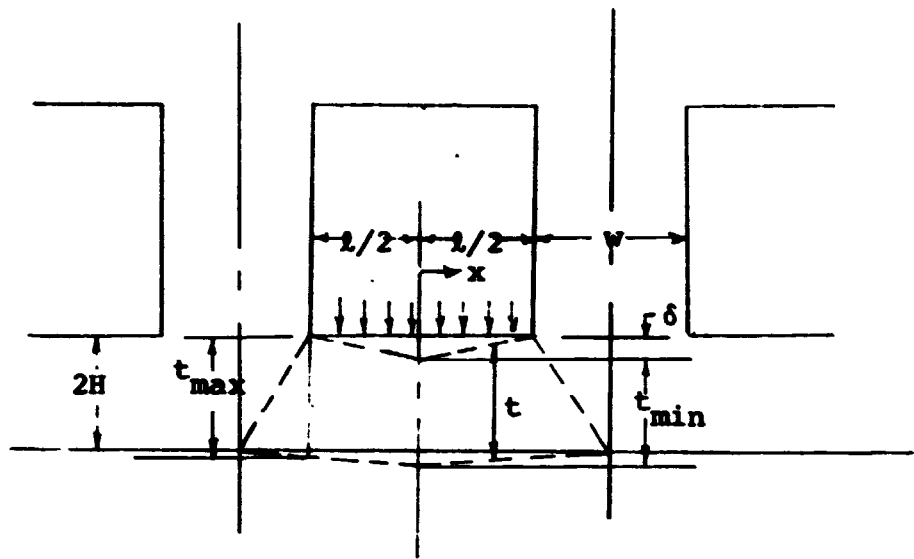
$$\gamma = 2 \left(2s - \frac{ms}{\sqrt{1-s^2}} \right) \frac{(\Delta\epsilon_{p_1})}{n} \quad (17)$$

The curvature and shear strain as determined from equations (15) and (17) for each cross section can then be integrated along the length of the ligament to obtain the bending and shear deflections. Once the total deflection is known, the corresponding thinning in the ligament is calculated by assuming that the volume of the material remains constant.

Experimental evidence shows that the deformed shape of the ligament can be approximated by a linear variation in thickness as shown in Figure 6. If δ denotes the deflection per cycle, the thinning after N cycles is then given by:

$$t_N = \frac{N \delta w}{(l + w)} \quad (18)$$

Note that even though the incremental deflection remains constant, the incremental strain at the center of the ligament increases with each cycle due to ligament thinning.



$$t(x) = (t_{\max} - t_{\min}) \frac{2x}{l} + t_{\min}$$

FIGURE 6 LIGAMENT LINEAR THINNING MODEL

3.5 Stress and Strain Resultants

The analysis of incremental plastic deformation involves generalized stresses m , n and s and the associated generalized strains. The generalized moment and shear and the generalized strain in the hoop direction are needed as input data for the solution. Their numerical values can be obtained by crude hand calculations using results of the thermal analysis and elastic finite element calculation or by performing the full inelastic analysis of the first two load cycles.

Hand Calculations

The bending moment distribution along the beam can be approximated by the solution for a clamped beam under uniformly distributed load:

$$M = \frac{-pl^2}{2} \left(\frac{1}{6} - \frac{x}{l} + \frac{x^2}{l^2} \right) \quad (19)$$

where p is the unit load, l is the length of the beam and x is the axial coordinate measured from the rib as shown in Figure A-1 of Appendix A.

Shear force is simply:

$$s = \frac{pl}{2} - px \quad (20)$$

The average hoop strain range, $\Delta\epsilon'_{P_1}$, in the ligament is evaluated based on the differential thermal expansion of the ligament at average temperature T_i and the closeout wall at average temperature T_o . Since the thickness of the ligament is small with respect to the thickness of the closeout wall, the elastic deformation of the closeout wall can be disregarded and the range of plastic strain in the hoop direction is:

$$\Delta \epsilon'_{p1} = \left[(T_i \alpha_i - T_o \alpha_o)_{\max} - (T_i \alpha_i - T_o \alpha_o)_{\min} \right] - (S_{y_{\max}} + S_{y_{\min}}) / E \quad (21)$$

where α_i and α_o are the thermal expansion coefficients of the ligament and closeout, respectively, and $(T_i \alpha_i - T_o \alpha_o)_{\max}$ and $(T_i \alpha_i - T_o \alpha_o)_{\min}$ are the maximum and minimum thermal strains, respectively, that occur during the loading cycle. $S_{y_{\max}}$ and $S_{y_{\min}}$ are respectively the ligament material absolute yield strengths corresponding to the ligament average temperatures at the times in the cycle when $(T_i \alpha_i - T_o \alpha_o)_{\max}$ and $(T_i \alpha_i - T_o \alpha_o)_{\min}$ are calculated.

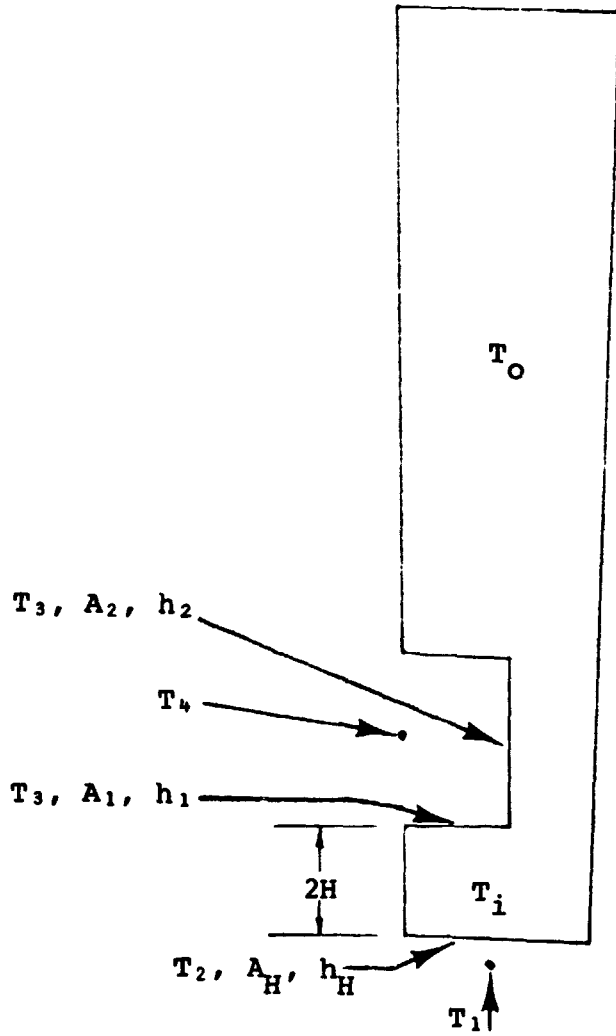
The average temperature of the ligament can be assessed assuming steady heat transfer conditions between the hot gas at adiabatic temperature and the evaporating hydrogen in the cooling channel.

Using a one dimensional heat flow model and assuming that heat enters the metal through the inner surface of the thrust chamber and is being received by two sides of the cooling channel as shown in Figure 7, the resulting temperature of the sides of the ligament are:

$$T_2 = \frac{\left(\frac{4H}{k} \frac{1}{A_H + A_1 + A_2} + \frac{1}{h_1 A_1 + h_2 A_2} \right) h_H A_H T_1 + T_4}{1 + h_H A_H \left[\frac{4H}{k} \frac{1}{A_H + A_1 + A_2} + \frac{1}{h_1 A_1 + h_2 A_2} \right]} \quad (22a)$$

$$T_3 = T_4 + \frac{h_H A_H}{h_1 A_1 + h_2 A_2} \left[T_1 - \frac{\left(\frac{4H}{k} \frac{1}{A_H + A_1 + A_2} + \frac{1}{h_1 A_1 + h_2 A_2} \right) h_H A_H T_1 + T_4}{1 + h_H A_H \left[\frac{4H}{k} \frac{1}{A_H + A_1 + A_2} + \frac{1}{h_1 A_1 + h_2 A_2} \right]} \right] \quad (22b)$$

where h and A denote heat transfer coefficients and surface areas as shown in Figure 7.



One Dimensional Heat Flow Model:

$$h_H A_H (T_1 - T_2) = \frac{k}{2H} \frac{A_H + A_1 + A_2}{2} (T_2 - T_3) = (h_1 A_1 + h_2 A_2) (T_3 - T_4)$$

FIGURE 7 THERMAL MODEL OF LIGAMENT

Thus the average temperature of the ligament is:

$$T_i = \frac{T_2 + T_3}{2} \quad (23)$$

A certain part of heat bypasses the cooling channel and heats the closeout wall, thus reducing the differential straining. The temperature of the closeout wall is approximately proportional to the average temperature of the ligament:

$$T_o = \bar{A} T_i \quad (24)$$

The approximate value of constant \bar{A} for the considered thrust chamber is 0.35. This value for \bar{A} was obtained for a specific geometry and will probably be different for other geometries.

The temperatures T_2 and T_3 can also be used to determine the thermally induced bending stress through the ligaments which for equibiaxial stress field is:

$$\sigma_b = \frac{\Delta T \alpha E}{2(1 - \nu)} \quad (25)$$

where ΔT is the temperature difference through the ligament.

Finite Element Thermal and Elastic Analyses

A more accurate evaluation of stress and strain resultants may be obtained by performing thermal and stress analyses for the extremal conditions using the finite element method. The formulation of the problem and instructions to prepare the input data for the MARC program are given in Appendix B. Selection of thermal steps is optimized by the program. The stress run should be performed for the instants resulting in the maximum range of

stress. The calculation of bending and shear tractions is straightforward. The plastic strain range in the hoop direction should be obtained by averaging the total strains through the thickness and correcting the result to account for elastic unloading as follows:

$$\Delta \epsilon_{p_1} = \Delta \epsilon_1 - \frac{(1 - \nu)}{E} (S_{y_{max}} + S_{y_{min}}) \quad (26)$$

In order to obtain conservative evaluation of plastic strain the correction for unloading derived by the second term in equation (26) is given for the equibiaxial state of stress.

The thermal bending through the wall should be evaluated by stress linearization.

Inelastic Solution for One or Two Cycles

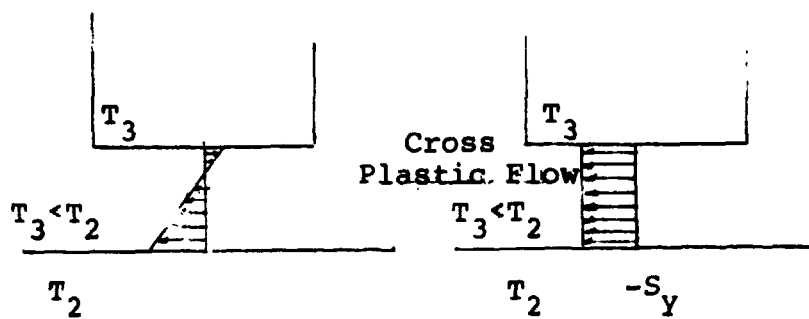
If better accuracy of the results is required, the resultants may be obtained by inelastic analysis of one or two cycles. The thermal analysis remains the same. Instructions for performing the inelastic stress and strain analyses using the MARC program are given in Appendix B. The program optimizes the load steps to obtain accurate results within the shortest computer time. As in elastic analysis, the bending and shear stress resultants are determined simply by linearizing the stresses through the thickness of the ligament. The range of plastic strain in the hoop direction is determined by adding absolute values of strains averaged through the thickness of the ligament within the entire cycle and taking half of the sum as a strain range, $\Delta \epsilon_{p_1}$.

3.6 Thermally Induced Stresses

The history of thermally induced stresses for the analyzed ligament is shown in Figure 8. As explained before, the ligaments are subjected to severe thermal straining due to the temperature difference between the outside and inside of the thrust chamber. As can be seen in Figure 3, there is also an essential temperature drop through the wall of the ligament. This causes bending since the ligament is constrained at the ends. The bending stress arises during the initial cooling phase, when the rapid chillover causes temperature gradients through the ligament. Tensile membrane stresses in the ligament exceed yield. The stresses increase until the temperature difference between the ligament and closeout wall reaches a maximum, after which unloading occurs. The stresses become compressive in the ligament in the residual state when a uniform temperature is attained.

Following ignition, the inner surface of the cylinder is subjected to intensive heat flux through the ligament. The temperature drop through the ligament results in thermally induced bending stresses. Compressive membrane stresses in the ligament exceed yield. Plastic flow in the hoop direction erases the effect of bending and the stresses remain essentially uniform through the ligament. Unloading occurs after the temperature difference between the ligament and closeout wall reaches a maximum and the stresses are relieved. The bending stresses generated in the ligament during unloading are again erased by straining in the hoop direction as the entire nozzle cools to a uniform temperature. The repetitive distribution of stress in subsequent cycles are illustrated in Figures 8a and b.

a) Beginning of Heat Transient Peak of Heat Transient



b) After Firing End of Transient

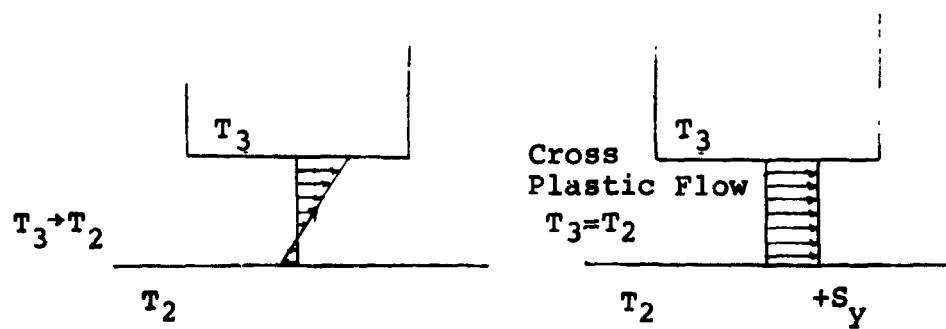


FIGURE 8 REPETITIVE CYCLE OF THERMALLY INDUCED BENDING STRESS IN LIGAMENT

The thermally induced bending though acting only for a short portion of the cycle, may enhance the ratcheting strain. Its effect may be assessed by computing the elastic energy of the thermally induced bending stresses and correcting the hoop strain accordingly.

The maximum thermal bending stress is given by equation (25), where ΔT is the temperature drop across the ligament. Thus, referring to Figure 9, the elastic energy is:

$$E_{el} = \frac{2}{E} \int_0^H \left(\sigma_b \frac{z}{H} \right)^2 dz \quad (27a)$$

$$= \frac{EH(\alpha \Delta T)^2}{6(1-\nu)^2} \quad (27b)$$

It is conservatively assumed that all of the available elastic energy goes into plastic straining of the ligament.

If $\Delta \epsilon_{p1}^*$ denotes the corresponding plastic hoop strain, then the plastic work is:

$$E_{pl} = 2 S_y \Delta \epsilon_{p1}^* H \quad (28)$$

Equating (27a) and (28):

$$\Delta \epsilon_{p1}^* = \frac{E(\alpha \Delta T)^2}{12(1-\nu)^2 S_y} \quad (29)$$

where S_y is the average of the absolute values of $S_{y_{max}}$ and $S_{y_{min}}$.

This must be added to the plastic strain range due to differential thermal expansion, $\Delta \epsilon_{p1}^*$, to obtain the plastic strain range in the hoop direction, $\Delta \epsilon_{p1}$.

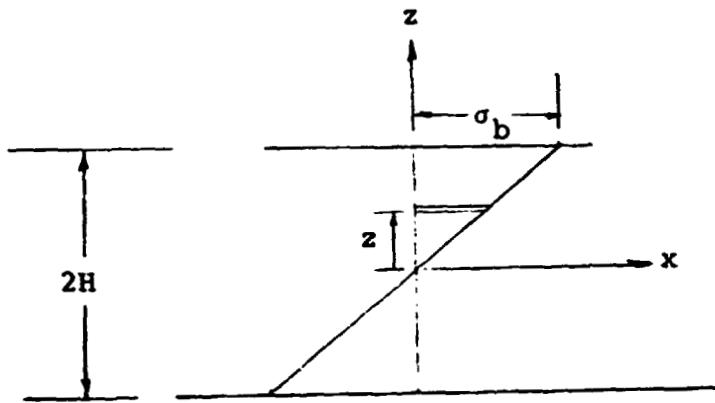


FIGURE 9 THERMAL BENDING IN LIGAMENT

4.0 DEVELOPMENT OF FAILURE MODE EVALUATION CRITERION

The ligaments are subjected to incremental plastic deformations during each firing cycle of the thrust chamber. The geometry of these ligaments changes as the incremental strains accumulate. They are subjected to incremental inward bending and simultaneously to a progressive thinning near the center of the ligament. Both fatigue damage and the tensile stability of the material are affected by local geometry changes.

Plastic tensile instability occurs when the incremental strain hardening of the deforming metal is less than the incremental increase of true stress due to local thinning. Once conditions of tensile instability are reached, further stretching occurs as minimum ligament section necking. The pressure in the chamber causes ultimate failure of the necked ligament.

4.1 Plastic Instability - Necking

The plastic tensile instability of the ligament in the displacement controlled thermal cyclic strain field is analyzed first by considering the ligament as a biaxially loaded shell subjected to monotonic tensile straining in the hoop and axial directions.

For a biaxially stretched sheet, the Mises yield condition is:

$$\bar{\sigma}^2 = \sigma_1^2 - \sigma_1\sigma_2 + \sigma_2^2 \quad (30a)$$

where $\bar{\sigma}$ is the effective stress and σ_1 and σ_2 are principal stresses in the hoop and axial directions, respectively.

Denoting the stress ratio $\frac{\sigma_1}{\sigma_2}$ by α , equation (30a) can be written as:

$$\bar{\sigma} = \sigma_1 (1 - \alpha + \alpha^2)^{1/2} \quad (30b)$$

In the present analysis elastic strains will be neglected and the Levy-Mises flow rule equations assumed to apply. The relation between the strain increments can then be written as [6]:

$$\frac{d\epsilon_1}{2\sigma_1 - \sigma_2} = \frac{d\epsilon_2}{2\sigma_2 - \sigma_1} = \frac{d\epsilon_3}{-\sigma_1 - \sigma_2} = \frac{d\bar{\epsilon}}{2\bar{\sigma}} \quad (31a)$$

where

$$d\bar{\epsilon} = \sqrt{\frac{2}{3}} \left(d\epsilon_1^2 + d\epsilon_2^2 + d\epsilon_3^2 \right)^{\frac{1}{2}} \quad (31b)$$

In the above, $d\bar{\epsilon}$ is the increment of effective strain and $d\epsilon_1$, $d\epsilon_2$ and $d\epsilon_3$ are the strain increments in the hoop, axial and radial (thickness) directions, respectively. Equation (31a) can be written in terms of α as:

$$\frac{d\epsilon_1}{2 - \alpha} = \frac{d\epsilon_2}{2\alpha - 1} = \frac{-d\epsilon_3}{1 + \alpha} = \frac{d\bar{\epsilon}}{2(1 - \alpha + \alpha^2)^{\frac{1}{2}}} \quad (31c)$$

For proportional loading the stress ratio remains constant and equation (31c) can be integrated to give the total strains:

$$\frac{\epsilon_1}{2 - \alpha} = \frac{\epsilon_2}{2\alpha - 1} = \frac{-\epsilon_3}{1 + \alpha} = \frac{\bar{\epsilon}}{2(1 - \alpha + \alpha^2)^{\frac{1}{2}}} \quad (31d)$$

Instability occurs when the hoop force F reaches a maximum, i.e.:

$$dF = d(2H a \sigma_1) = 0 \quad (32)$$

where $2H$ denotes the thickness of the ligament and a its

axial length. Equation (32) is differentiated to give:

$$\frac{d\sigma_1}{\sigma_1} = -\frac{da}{a} - \frac{dH}{H}$$

$$\frac{d\sigma_1}{\sigma_1} = -d\epsilon_2 - d\epsilon_3 \quad (33)$$

From the incompressibility condition of plastically deformed material:

$$d\epsilon_1 + d\epsilon_2 + d\epsilon_3 = 0 \quad (34a)$$

or

$$d\epsilon_1 = -d\epsilon_2 - d\epsilon_3 \quad (34b)$$

For proportional loading:

$$\frac{d\sigma_1}{\sigma_1} = \frac{d\bar{\sigma}}{\bar{\sigma}} \quad (35)$$

Thus, equation (33) becomes:

$$\frac{d\bar{\sigma}}{\bar{\sigma}} = d\epsilon_1 \quad (36)$$

Using the flow law equation (31c), the condition for instability is given by:

$$\frac{d\bar{\sigma}}{d\epsilon} = \frac{(2-a)\bar{\sigma}}{2(1-a+a^2)^{\frac{1}{2}}} \quad (37)$$

If the stress-strain law is given by:

$$\bar{\sigma} = A\bar{\epsilon}^n \quad (38)$$

where A and n are material constants, then on differentiating:

$$\begin{aligned}\frac{d\bar{\sigma}}{d\bar{\epsilon}} &= \frac{n\bar{\sigma}}{\bar{\epsilon}} \\ \frac{d\bar{\sigma}}{d\bar{\epsilon}} &= \frac{\bar{\sigma}}{z}\end{aligned}\quad (39)$$

where $z = \bar{\epsilon}/n$ is the subtangent in Figure 10.

From equations (37) and (39):

$$z = \frac{2(1 - \alpha + \alpha^2)^{\frac{1}{2}}}{(2 - \alpha)} \quad (40)$$

and the critical effective strain is:

$$\bar{\epsilon}_{cr} = \frac{2n(1 - \alpha + \alpha^2)^{\frac{1}{2}}}{(2 - \alpha)} \quad (41)$$

The critical strain in the minimum ligament section from equation (31d) is then:

$$\epsilon_{1 cr} = n \quad (42)$$

For cyclic loading, the compressive straining of a ligament at the beginning of the loading cycle is followed by tensile strains. In each loading cycle the ligament accumulates plastic strain. The net increments in the hoop and radial directions occur at the end of the cycle when the axial strain is zero. Thus, the limits of material stability can be approximated by the analysis for plane strain conditions. The plastic strains in the

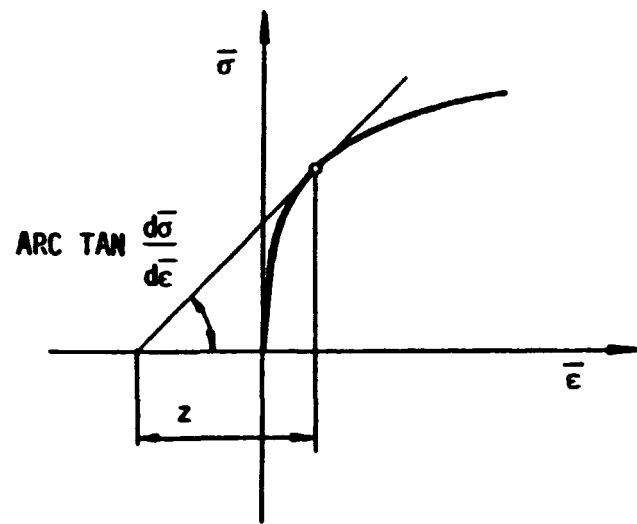


FIGURE 10 - CONSIDERE'S CONSTRUCTION

hoop direction $d\epsilon_1$, and in the radial direction $d\epsilon_3$ satisfy the condition of incompressibility. Since $d\epsilon_2 = 0$:

$$d\epsilon_1 = -d\epsilon_3 \quad (43)$$

Now,

$$\epsilon_3 = \ln\left(\frac{t}{2H}\right) \quad (44)$$

where $2H$ denotes the original ligament thickness and t the ligament variable thickness. Then using equations (42), (43) and (44), the critical thickness at instability is given by:

$$t_{cr} = 2H e^{-\epsilon_1} \quad (45)$$

$$t_{cr} = 2H e^{-n} \quad (46)$$

4.2 Strain Range - Fatigue

For fatigue calculations, the maximum local hoop strain range at the minimum ligament section can be obtained from the average hoop strain range by integration if the geometry of the distorted ligament is known. As mentioned earlier, tests indicate that the deformed shape of the ligament can be approximated by a linear function as shown in Figure 6. Thus, the thickness variation can be written as:

$$t(x) = \left(t_{\max} - t_{\min}\right) \frac{2x}{l} + t_{\min} \quad (47)$$

where t_{\max} and t_{\min} are as shown in the figure. Now, the average strain in the hoop direction is given by:

$$\epsilon_{1 \text{ avg}} = \frac{2}{l} \int_0^{l/2} \epsilon_1(x) dx \quad (48)$$

From equilibrium of forces in the hoop direction:

$$\sigma_1(x) t(x) = \sigma_{1 \text{ min}} t_{\text{min}} \quad (49)$$

Using the yield condition equation (30b), since α is constant equation (49) becomes:

$$\bar{\sigma}(x) t(x) = \bar{\sigma}_{\text{min}} t_{\text{min}} \quad (50)$$

Substituting the stress-strain law, equation (38):

$$\bar{\epsilon}(x)^n t(x) = \bar{\epsilon}_{\text{min}}^n t_{\text{min}} \quad (51)$$

Now making use of the flow law, equation (31d) for constant α :

$$\epsilon_1(x)^n t(x) = \epsilon_{1 \text{ min}}^n t_{\text{min}} \quad (52)$$

Substituting for $\epsilon_1(x)$ into equation (48), the relation between the average strain and local strain is given by:

$$\epsilon_{1 \text{ avg}} = \frac{2\epsilon_{1 \text{ min}}}{l} \int_0^{l/2} \left\{ \frac{t_{\text{min}}}{t(x)} \right\}^{1/n} dx \quad (53a)$$

Substituting for $t(x)$ from equation (47) and integrating:

$$\epsilon_{1 \text{ avg}} = \epsilon_{1 \text{ min}} \frac{n}{n-1} \frac{t_{\text{min}}}{(t_{\text{max}} - t_{\text{min}})} \left[\left(\frac{t_{\text{max}}}{t_{\text{min}}} \right)^{\frac{n-1}{n}} - 1 \right] \quad (53b)$$

or

$$\epsilon_{1\min} = \epsilon_{1\text{avg}} \left(\frac{n-1}{n} \right) \left(\frac{t_{\max}}{t_{\min}} - 1 \right) / \left[\left(\frac{t_{\max}}{t_{\min}} \right)^{\frac{n-1}{n}} - 1 \right] \quad (53c)$$

As the deformation increases with each cycle, the thicknesses t_{\max} and t_{\min} also change per cycle. This, in turn, changes $\epsilon_{1\min}$, the local strain in the minimum ligament section which intensifies with each cycle.

The axial strain in the minimum ligament section is given by:

$$\epsilon_{2\min} = \alpha(T_i - T_o) \quad (54a)$$

Also, from the condition of incompressibility:

$$\epsilon_{3\min} = -(\epsilon_{1\min} + \epsilon_{2\min}) \quad (54b)$$

Now the effective strain range in the minimum ligament section for entering the fatigue curve is:

$$\bar{\epsilon}_{\min} = \frac{\sqrt{2}}{3} \sqrt{(\epsilon_{1\min} - \epsilon_{2\min})^2 + (\epsilon_{1\min} - \epsilon_{3\min})^2 + (\epsilon_{2\min} - \epsilon_{3\min})^2} \quad (55a)$$

Substituting equation (54b) into (55a):

$$\begin{aligned} \bar{\epsilon}_{\min} &= \frac{\sqrt{2}}{3} \sqrt{(\epsilon_{1\min} - \epsilon_{2\min})^2 + (2\epsilon_{1\min} + \epsilon_{2\min})^2 + (2\epsilon_{2\min} + \epsilon_{1\min})^2} \\ &= \frac{2}{\sqrt{3}} \sqrt{\epsilon_{1\min}^2 + \epsilon_{1\min}\epsilon_{2\min} + \epsilon_{2\min}^2} \quad (55b) \end{aligned}$$

For the linear variation assumed, the thickness t_{\min} and t_{\max} after the N^{th} cycle are given by:

$$t_{\min} = \frac{2H(\ell + w) - N \delta w}{(\ell + w)} \quad (56a)$$

$$t_{\max} = \frac{2H(\ell + w)^2 + N \delta \ell w}{(\ell + w)^2} \quad (56b)$$

where δ is the deformation per cycle.

Equations (55) and (56) along with the fatigue curve can be used to determine the fatigue life. However, since $\epsilon_{1\min}$ changes with each cycle, a numerical procedure is necessary for performing the calculations to determine fatigue life. A FORTRAN program has been written for determining the cycles to failure and is included in Appendix C.

5.0 THRUST CHAMBER LIFE PREDICTIONS

The results obtained using the analyses described can be used to determine the life of the thrust chamber. For small ligament distortion it can be conservatively assumed that the incremental thinning of the ligament remains constant during subsequent cycles. The number of cycles to failure can then be bounded from below by considering the number of cycles needed to reduce the thickness of the ligament below the critical value resulting in tensile instability or by considering the fatigue damage of the gradually thinned ligament, whichever results in smaller number of cycles. For OFHC copper this bounding technique provides a realistic evaluation of the cycles to failure observed in experiments where failure was due to tensile instability.

For NARloy Z the thinning gradually diminishes in consecutive cycles and the fatigue mode of failure prevails. This bounding technique provides a conservative evaluation. However, the efficiency of the bound is significantly lower than for copper.

The tendency of diminishing increments of accumulated strain in consecutive cycles is the result of kinematic hardening. It has been demonstrated [7], [8], that for such material the cyclically loaded structure always achieves the condition of alternating plastic straining if there is no limit on the hardening capacity and the changes of geometry can be ignored. The net increment of plastic ratchet strain vanishes after sufficient hardening. The amount of plastic strain accumulation needed to achieve such plastic shakedown can be uniquely determined. For real materials with limited hardening capacity and less than ideal kinematic behavior, the stable cyclic state occurs at much larger accumulated strains than for an ideal kinematically hardening material or may never be achieved. Materials more closely obeying the theoretical concept of kinematic hardening can be expected to fail due to fatigue since slowed down thinning allows the material to be exposed to more fatigue cycles, as in the case of NARloy Z.

This trend is also in general agreement with the results of [9]. The number of cycles at which thinning stops is related to the strain hardening parameter n . Assuming this to be the dominating parameter on which the number of cycles to thinning depend and hypothesizing a power relationship, the following empirical criterion is obtained:

$$N_T = 750n^{1.25} \quad (57)$$

where N_T denotes the number of cycles at which thinning stops.

Note that the results of [9] have been partly used in determining the constants for the power relationship since these were the only quantifiable numbers available.

If the number of cycles to reach the critical thickness obtained from plastic instability analysis is less than N_T for that material, then tensile stability is the limiting failure mode. The thrust chamber life in this case is given by the number of cycles to instability. If on the other hand, N_T is greater, fatigue is the failure mode and thrust chamber life is given by N_T plus the cycles obtained from the fatigue curve corresponding to the effective strain range which remains constant from that point on.

The numerical calculations for the case of OFHC copper and NARloy Z using the procedure developed herein are presented in Appendix A.

6.0 FINITE ELEMENT ANALYSIS

The MARC program was used for the thermal and mechanical part of the analysis. The MARC program was adapted to analyze the fast thermal and pressure thrust nozzle transient. Optimized selection of the time and load steps was used for the thermal and elastic-plastic analyses.

The finite element inelastic analysis confirmed the fact that the simplified model includes the essence of the physical behavior of the ligament as described herein during the course of the development procedure. Moreover, the results of the finite element analysis were employed in deriving and calibrating the thermal model of the ligament. A description of the model and details of the finite element analysis for the case of OFHC copper are given in Appendix B.

7.0 COMPARISON OF RESULTS

The numerical results obtained for OFHC copper, using the simplified analysis procedure developed herein, are compared with the finite element results in Table 1. The results are seen to be in good agreement. The life prediction of 103 cycles for OFHC copper and 833 cycles for NARloy Z is also in general agreement with experimental results [2] indicating that the simplified design procedure can be used for predicting the life of the thrust chamber without performing detailed inelastic analysis.

TABLE 1

Comparison of Analytical vs. Finite Element Results
Residual Deflection After One Cycle

Analytical Results	Finite Element Results
Deflection of Pressure Surface/Cycle	Deflection of Pressure Surface/Cycle
.00029" (.00737 mm)	.00027" (.00686 mm)

8.0 CONCLUSIONS

A simplified design procedure for predicting thrust chamber life is developed herein. The method uses a yield surface for combined bending and membrane loading to determine the incremental inward bulging and progressive thinning near the center of the ligaments at the inner liner of the thrust chamber. Failure analyses indicate that plastic tensile instability is the dominant mode of failure for OFHC copper. Both fatigue and plastic tensile instability must be analyzed for NARloy Z to determine the limiting failure mode. Results of the

simplified analyses are shown to compare favorably with those obtained from detailed inelastic finite element analyses for OFHC copper.

Further experiments are needed to provide better characterization of plastic response of the materials used for thrust chambers.

For longer cycle times, the accuracy of the evaluation can be improved by including the time dependent response of the material into the analysis.

9.0 REFERENCES

1. Hannum, N.P., Kasper, H.J., Pavli, A.J., "Experimental and Theoretical Investigation of Fatigue Life in Reusable Rocket Thrust Chambers," NASA TM X-73413, Lewis Research Center, Cleveland, Ohio, July 1976.
2. Quentmeyer, R.J., "Experimental Fatigue Life Investigation of Cylindrical Thrust Chambers," NASA TM X-73665, Lewis Research Center, Cleveland, Ohio, July 1977.
3. Esposito, J.J., Zabora, R.F., "Thrust Chamber Life Prediction - Mechanical and Physical Properties of High Performance Rocket Nozzle Materials," NASA CR-134806, Contract NAS3-17838, NASA-Lewis Research Center, Cleveland, Ohio, March 1975.
4. Hodge, P.G., Jr., "Plastic Analysis of Structures," McGraw Hill Book Co., 1959.
5. Peterson, D.B., Kroenke, W.C., Stokey, W.F., O'Donnell, W.J., "Generalized Yield Surfaces for Plates and Shells," WRC Bulletin No. 250, July 1979.
6. Johnson, W., Mellor, P.B., "Engineering Plasticity," Van Nostrand Reinhold Co., 1973.
7. Frederick, C. O., Armstrong, P. J., "Convergent Internal Stresses and Steady Cyclic States of Stress," Jnl. of Strain Analysis, Vol. 1, p. 154 (1966).
8. Halphen, M. B., "L'accommodation des structures elasto-plastiques a ecrouissage cinematique," C. R. Acad. Sc. Paris, t. 283 A, p. 799 (1976).
9. Armstrong, W. H., "Structural Analysis of Cylindrical Thrust Chamber," Final Report Volume II, NASA CR-165241, Contract NAS3-21953, NASA-Lewis Research Center, Cleveland, Ohio, March 1981.

APPENDIX A
NUMERICAL EXAMPLES

Example I

Consider the ligament for OFHC copper. The geometry is as shown in Figure A-1.

For a unit width of the ligament $\Delta p = 547 \text{ lb/in. (95794.47 N/m)}$

The average yield stress $S_y = 9000 \text{ psi. (62 MPa)}$

Then from elastic solution for a clamped beam (eqs. (19) and (20))

$$\text{Moment} \quad M = \frac{-p\ell^2}{2} \left(\frac{1}{6} - \frac{x}{\ell} + \frac{x^2}{\ell^2} \right)$$

$$\text{Shear Force} \quad S = \frac{p\ell}{2} - px$$

From eq. (3a):

$$\text{Yield Moment} \quad M_o = H^2 S_y$$

$$\therefore \text{From eq. (2a):} \quad m = \frac{M}{M_o}$$

$$m = \frac{-547 \cdot (.0664)^2}{2 \cdot \left(\frac{.035}{2}\right)^2 \cdot 9000} \left[\frac{1}{6} - \frac{x}{.0664} + \frac{x^2}{(.0664)^2} \right]$$

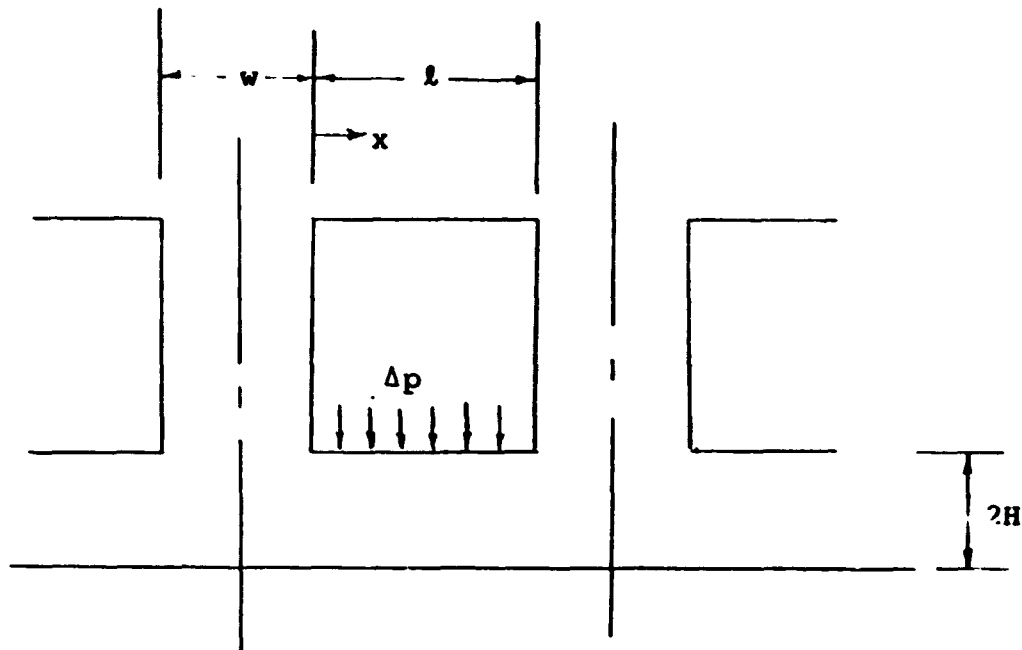
$$m = -0.0729 + 6.5888x - 99.229x^2 \quad (\text{A-1})$$

From eq. (10b):

$$s = \frac{S}{H S_y}$$

$$s = \frac{1}{\left(\frac{.035}{2}\right) \cdot 9000} \left(\frac{547 \cdot .0664}{2} - 547x \right)$$

$$= .1153 - 3.473x \quad (\text{A-2})$$



$$\begin{aligned}
 l &= 0.0664'' \quad (1.686 \text{ mm}) \\
 2H &= 0.035'' \quad (0.889 \text{ mm}) \\
 w &= 0.05'' \quad (1.27 \text{ mm})
 \end{aligned}$$

FIGURE A-1 GEOMETRY OF OFHC LIGAMENT

From eq. (6b):

$$\begin{aligned} k &= \sqrt{1 - s^2} \\ &= (.9867 + .8009x - 12.062x^2)^{\frac{1}{2}} \end{aligned} \quad (\text{A-3})$$

From eq. (6a) the yield surface:

$$\begin{aligned} F &= m + \frac{n^2}{k} - k = 0 \\ n^2 &= k^2 - km \end{aligned} \quad (\text{A-4a})$$

Substituting eqs. (A-1) and (A-3):

$$\begin{aligned} n &= \left[.9867 + .8009x - 12.062x^2 \right. \\ &\quad \left. - (.9867 + .8009x - 12.062x^2)^{\frac{1}{2}} \right. \\ &\quad \left. (- .0729 + 6.5888x - 99.229x^2) \right]^{\frac{1}{2}} \end{aligned} \quad (\text{A-4b})$$

From eq. (21), taking $\alpha_i = \alpha_o = \alpha$ and $(S_{y_{\max}} + S_{y_{\min}})/2 = S_y$, the plastic strain range in the hoop direction is:

$$\Delta \epsilon_{P_1}' = \left[\alpha \left\{ (T_i - T_o)_{\max} - (T_i - T_o)_{\min} \right\} - \frac{2 S_y}{E} \right] \quad (\text{A-5a})$$

From thermal analysis, $[(T_i - T_o)_{\max} - (T_i - T_o)_{\min}] \approx 780^\circ\text{F}$ (433°K)

Then for $\alpha = 9.5 \times 10^{-6}$ in./in./ $^\circ\text{F}$, (17.1×10^{-6} $^\circ\text{C}^{-1}$) and $E = 17 \times 10^6$ psi (117215 MPa):

$$\begin{aligned} \Delta \epsilon_{P_1}' &= \left[9.5 \cdot 10^{-6} \cdot 780 - \frac{2 \cdot 9000}{17 \cdot 10^6} \right] \\ \Delta \epsilon_{P_1}' &= 0.00635 \end{aligned}$$

From eq. (29):

$$\Delta \epsilon_{P_1}^{\bullet} = \frac{E \alpha^2 (\Delta T)^2}{12(1-\nu)^2 S_y} \quad (\text{A-5b})$$

The temperature drop across the ligament $\Delta T = 200^\circ\text{F}$:

$$\Delta \epsilon_{P_1}^{\bullet} = \frac{17 \cdot 10^6 \cdot (9.5)^2 (10^{-6})^2 (200)^2}{12(1-0.3)^2 \cdot 9000}$$

$$\Delta \epsilon_{P_1}^{\bullet} = .00116$$

$$\therefore \Delta \epsilon_{P_1} = \Delta \epsilon_{P_1}^{\prime} + \Delta \epsilon_{P_1}^{\bullet} = .00751 \quad (\text{A-6})$$

From eqs. (6b) and (15):

$$K = \frac{2k}{n} \frac{(\Delta \epsilon_{P_1})}{H} \quad (\text{A-7})$$

For the present problem, m and s are small compared to n . Thus it is found from equation (A-4a) that $n \approx k$. Eq. (A-7) then simplifies to:

$$K = \frac{2(\Delta \epsilon_{P_1})}{H} \quad (\text{A-8})$$

$$\therefore K = \frac{1}{R} = \frac{2(.00751)}{.0175}$$

where the radius R is assumed for the length shown in Figure A-2.

Thus $R = 1.1651''$ (29.59 mm)

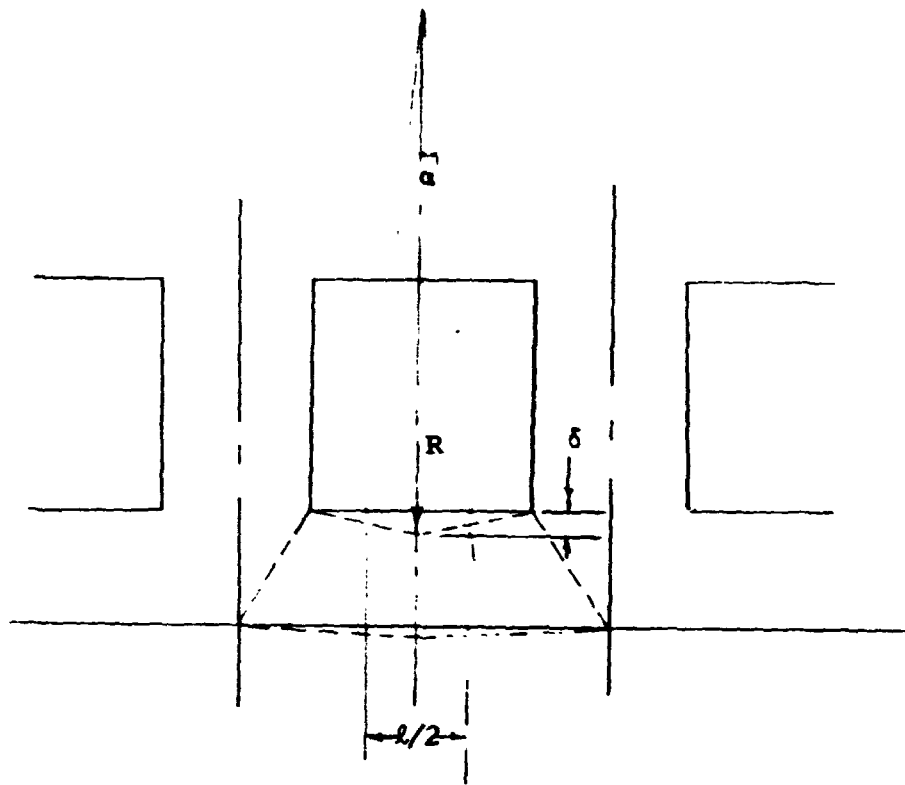


FIGURE A-2 DEFORMED LIGAMENT

$$\begin{aligned} \therefore \text{Deflection } \delta_1 &= 2R(1 - \cos \alpha) \\ &= 2(1.1651) \left[1 - \left\{ (1.1651)^2 - (.0166)^2 \right\}^{1/2} / 1.1651 \right] \end{aligned}$$

$$\therefore \delta_1 = .0002365'' \quad (.006 \text{ mm})$$

From eq. (17), since the contribution of m and s is small, the product term $\frac{ms}{\sqrt{1-s^2}}$ can be neglected and n taken = 1 as seen from Fig. 5b.

$$\text{Thus:} \quad \gamma = 4s \left(\Delta \epsilon_{P_1} \right) \quad (\text{A-9})$$

Substituting from eqs. (A-2) and (A-6):

$$\begin{aligned} \gamma &= 4(0.1153 - 3.473x)(.00751) \\ \gamma &= .003464 - 0.104328x \end{aligned} \quad (\text{A-10})$$

Integrating and determining the deflection at $x = l/2$:

$$\begin{aligned} \delta_2 &= .003464x - 0.104328x^2/2 \\ \delta_2 &= 0.0000575'' \quad (.0015 \text{ mm}) \end{aligned}$$

$$\therefore \text{Total } \delta = \delta_1 + \delta_2 = .000294'' \quad (.0075 \text{ mm})$$

From eq. (18), thinning after N cycles:

$$t_N = \frac{0.000294 \cdot 0.05N}{(0.0664 + 0.05)}$$

$$\therefore t_N = 0.0001263N \text{ inches} \quad (\text{A-11})$$

Material Instability

The strain hardening parameter n in the stress-strain law is approximately given by LeRC as:

$$n = 0.2 \left(\frac{S_u - S_y}{S_y} \right)^{0.6}$$

where S_u denotes the ultimate strength and S_y the yield strength.

Towards the end of the cycle, the value of S_u and S_y are approximately 46 ksi (317 MPa) and 9 ksi (62 MPa), respectively. Thus:

$$\begin{aligned} n &= 0.2 \left(\frac{46 - 9}{9} \right)^{0.6} \\ &= 0.467 \end{aligned}$$

From Eq. (46), critical thickness for $n = 0.467$

$$t_{cr} = (0.035)e^{-0.467}$$

$$t_{cr} = 0.02194" \quad (.557 \text{ mm})$$

$$\begin{aligned} \therefore \text{Thinning for} \\ \text{Instability} &= (.035 - .02194) \\ &= .01306" \quad (0.332 \text{ mm}) \end{aligned} \quad (\text{A-12})$$

Equating (A-11) and (A-12), the number of cycles to instability are:

$$N = 103$$

From equation (57)

$$\begin{aligned} N_T &= 750 (0.467)^{1.25} \\ &= 289 \text{ cycles} \end{aligned}$$

Thus thinning continues for 289 cycles.

Since $N < N_T$, the failure mode is material instability and thrust chamber life equals 103 cycles.

Fatigue

To demonstrate that fatigue results in a higher number of cycles, the procedure described in Section 4.2 was used to

determine the fatigue life of the OFHC ligament. The fatigue life was based on the fatigue curve for OFHC copper shown in Figure A-3. The calculations were performed using the FORTRAN program listed in Appendix C. The fatigue life was determined to be 132 cycles.

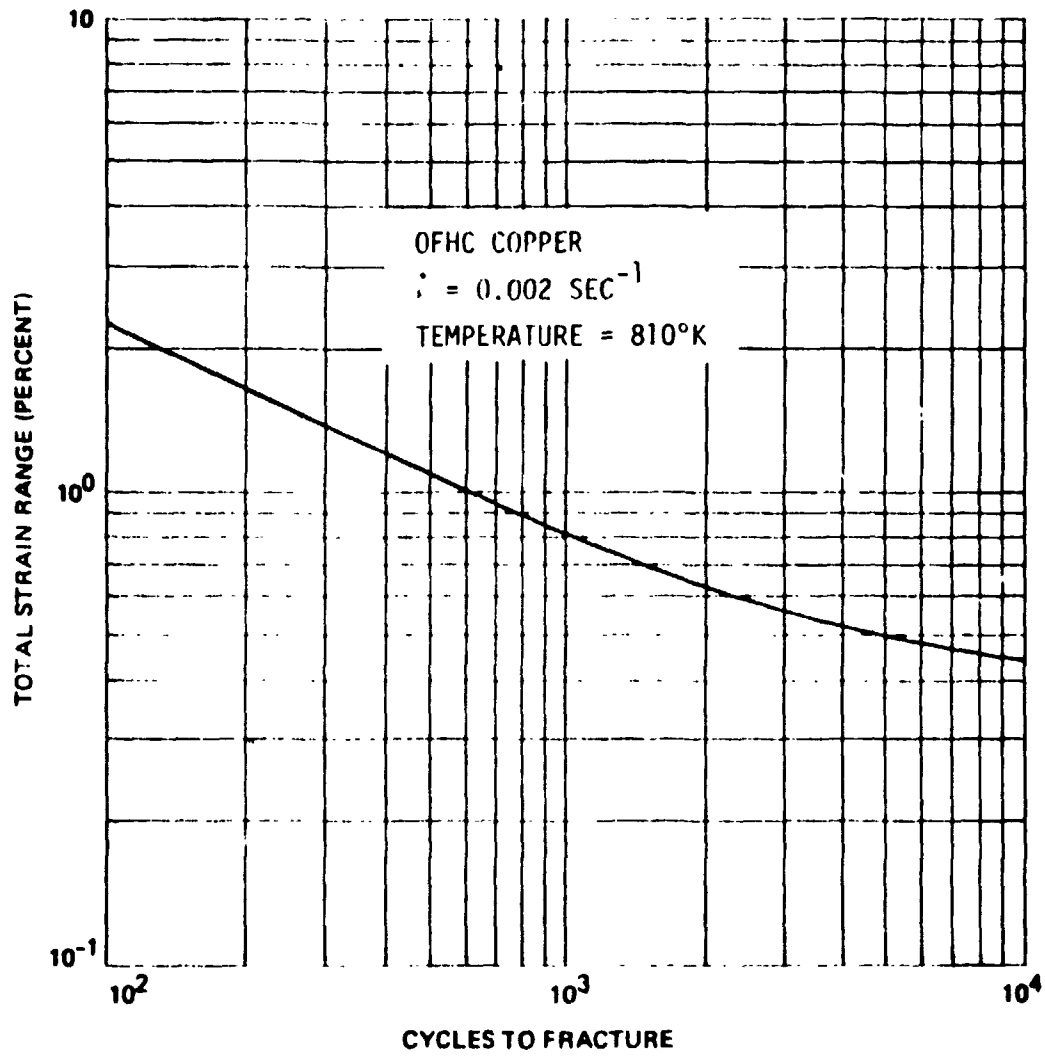


FIGURE A-3 TYPICAL LOW-CYCLE FATIGUE LIFE OF OFHC COPPER ANNEALED CONDITION

Example II:

Consider now an example of NARloy Z. The geometry is the same as shown in Figure A-1

Also, $\Delta p = 547 \text{ lb/in.}$ (95794.47 N/m)

The average yield stress $S_y = 30,000 \text{ psi}$ (207 MPa)

As before, from Eq. (21)

$$\Delta \epsilon'_{P_1} = \alpha \left\{ (T_i - T_o)_{\max} - (T_i - T_o)_{\min} \right\} - \frac{2 S_y}{E} \quad (\text{A-13})$$

Since the thermal conductivity for NARloy Z is approximately the same as that of OFHC copper, temperatures T_i and T_o are approximately the same.

Then for $\alpha = 9.5 \times 10^{-6} \text{ in./in./}^\circ\text{F}$, ($17.1 \times 10^{-6} \text{ }^\circ\text{C}^{-1}$) and $E = 18 \times 10^6 \text{ psi}$ (124110 MPa):

$$\Delta \epsilon'_{P_1} = 9.5 \cdot 10^{-6} \cdot 780 - \frac{2 \cdot (30000)}{18 \cdot 10^6}$$

$$\therefore \Delta \epsilon'_{P_1} = .004077$$

From Eq. (29)

$$\Delta \epsilon''_{P_1} = \frac{18 \cdot 10^6 \cdot (9.5)^2 (10^{-6})^2 (200)^2}{12(1-0.3)^2 \cdot 30000}$$

$$\therefore \Delta \epsilon''_{P_1} = .000368$$

$$\therefore \Delta \epsilon_{P_1} = \Delta \epsilon'_{P_1} + \Delta \epsilon''_{P_1} = .004445$$

Substituting in :

$$K = \frac{2(\Delta \epsilon_{P_1})}{H}$$

$$K = \frac{1}{R} = \frac{2(.004445)}{.0175}$$

$$\therefore R = 1.9685" \quad (50 \text{ mm})$$

$$\therefore \text{Deflection } \delta_1 = 2R(1-\cos\alpha) = .00014" \quad (.0035 \text{ mm})$$

From Eq. (10b) and (20)

$$s = \frac{S}{HS_y}$$

$$\therefore s = \frac{1}{\frac{.035}{2} \cdot 30000} \left(\frac{547 \cdot 0.0664}{2} - 547x \right)$$

$$= 0.0346 - 1.042x \quad (\text{A-14})$$

Substituting in:

$$\gamma = 4s(\Delta\epsilon_{P_1})$$

$$\therefore \gamma = 4(.0346 - 1.042x)(.004445)$$

$$= 0.000615 - 0.018527x \quad (\text{A-15})$$

Integrating and determining the deflection at $x=l/2$

$$\delta_2 = 0.00001" \quad (.000254 \text{ mm})$$

$$\therefore \text{Total } \delta = \delta_1 + \delta_2 = 0.00015" \quad (.00381 \text{ mm})$$

From Eq. (18), thinning after N cycles:

$$t_N = \frac{0.00015 \cdot 0.05N}{(0.0664 + 0.05)}$$

$$\therefore t_N = 0.0000644 N \text{ inches} \quad (\text{A-16})$$

Material Instability

For $S_u = 55 \text{ ksi}$ (379 MPa) and $S_y = 30 \text{ ksi}$ (207 MPa)

$$n = 0.2 \left(\frac{55-30}{30} \right)^{0.6}$$

$$\therefore n = 0.18$$

From Eq. (46)

$$t_{cr} = (.035)e^{-0.18}$$

$$= 0.0292" \quad (.742 \text{ mm})$$

$$\therefore \text{Thinning for instability} = 0.035 - 0.0292$$

$$= 0.0058" \quad (.147 \text{ mm}) \quad (\text{A-17})$$

Equating (A-16) and (A-17), the number of cycles to instability

$$N = 90$$

From Eq. (57)

$$\begin{aligned} N_T &= 750(0.18)^{1.25} \\ &= 98 \end{aligned}$$

Thus thinning stops after 88 cycles.

Since $N > N_T$, material instability is not the failure mode and the thrust chamber life must be determined from fatigue calculations.

Fatigue

The procedure of Section 4.2 was used for determining the fatigue life of NARloy Z. The fatigue life was based on the fatigue curve of Figure A-4. The FORTRAN Program listed in Appendix C was used for performing the necessary calculations. The input and output obtained are attached in this Appendix. The notation for the listed results is as follows:

- NCYC - Number of cycles
- TMIN - t_{\min} , minimum ligament thickness - in.
- TMAX - t_{\max} , maximum ligament thickness - in.
- EEQVT - effective strain range %
- NF - Number of cycles to failure from fatigue curve
- USEAGE- Usage factor

Thus if the ligament were to continue thinning, the fatigue life would be 272 cycles. However since thinning stops after 88 cycles, the remaining fatigue life is based on the effective strain range of 2.2416% which now remains constant and equals 747 cycles.

$$\begin{aligned} \text{Thus cycles to failure} &= 88 + 747 \\ &= 835 \end{aligned}$$

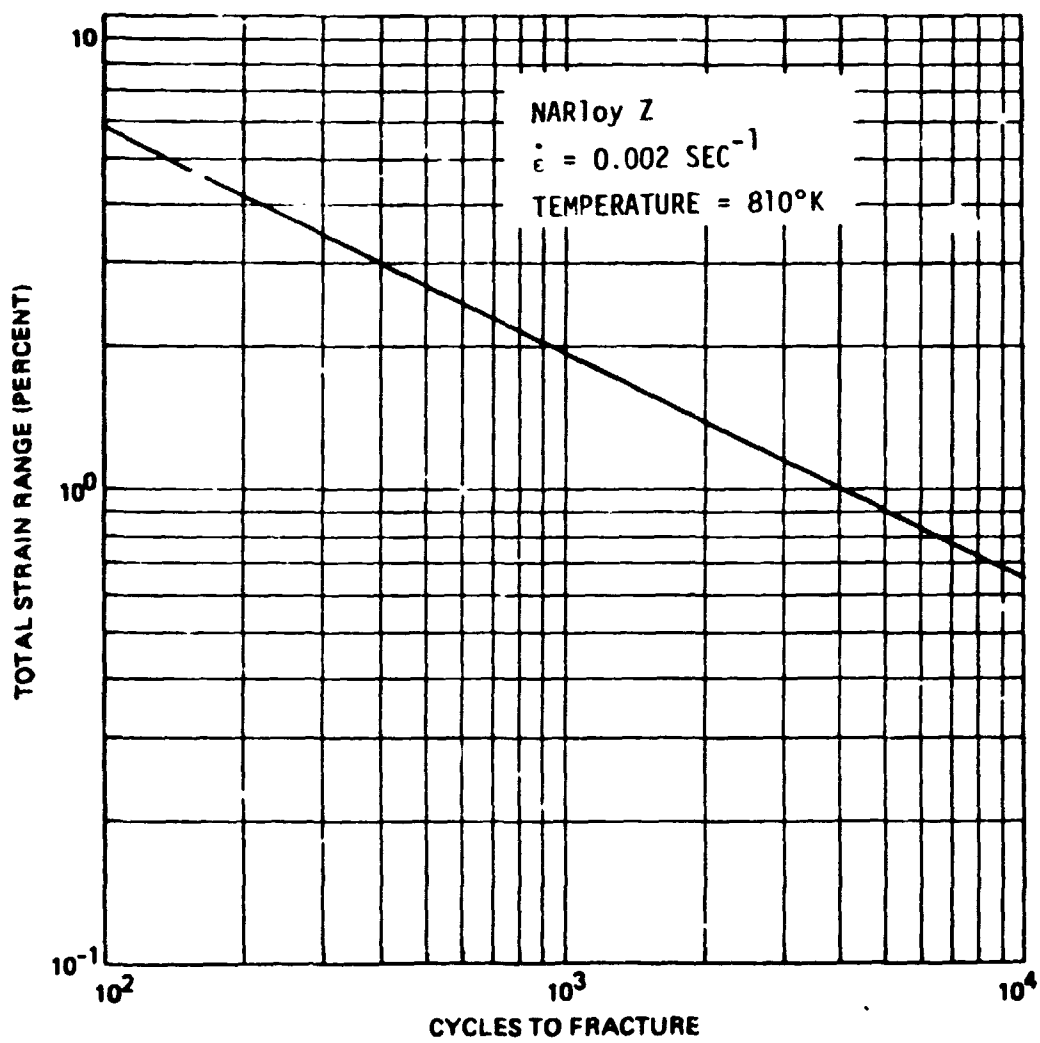


Figure A-4 Typical Low-Cycle Fatigue Life of NARloy Z

CONSTANTS INPUT

NARloy-Z

N= .18000 - n (material strain hardening exponents)
 DELTA= .15000E-03 - δ (Deflection per cycle, in.)
 E1AVG= .74100% - $\epsilon_{1_{avg}}$ (Average hoop strain in ligament, $\alpha\Delta T$) = $\epsilon_{2_{min}}$.
 H= .17500E-01 - half ligament thickness, in.
 L= .66400E-01 - l (width of ligament in hoop direction, in.)
 W= .50000E-01 - w (width of rib, in.)

FATIGUE CURVE

CYCLES	STRAIN RANGE
10.000	18.000
100.00	5.9000
4000.0	1.0000
.50000E+06	.10000

RESULTS FOR FACT CYCLE IN CYC, TMIN, TMAX, FEQVT, NF, USEAGE

1	.34036E-01	.35037F-01	1.4880	1751.3	.57101E-03
2	.34071E-01	.35074F-01	1.4940	1736.0	.11468E-02
3	.34107E-01	.35110F-01	1.5001	1722.0	.17276E-02
4	.34142E-01	.35147F-01	1.5062	1707.5	.23132E-02
5	.34178E-01	.35184F-01	1.5124	1693.0	.29039E-02
6	.34213E-01	.35221F-01	1.5186	1678.0	.34946E-02
7	.34249E-01	.35257F-01	1.5249	1664.3	.41004E-02
8	.34285E-01	.35294F-01	1.5312	1650.0	.47065E-02
9	.34320E-01	.35331F-01	1.5376	1635.0	.53178E-02
10	.34356E-01	.35368F-01	1.5441	1621.0	.59345E-02
11	.34391E-01	.35404F-01	1.5506	1607.5	.65566E-02
12	.34427E-01	.35441F-01	1.5571	1593.5	.71841E-02
13	.34462E-01	.35478F-01	1.5637	1579.5	.78172E-02
14	.34498E-01	.35515F-01	1.5704	1565.7	.84559E-02
15	.34534E-01	.35551F-01	1.5771	1551.0	.91003E-02
16	.34569E-01	.35588F-01	1.5839	1536.1	.97505E-02
17	.34605E-01	.35625F-01	1.5907	1524.4	.10406E-01
18	.34640E-01	.35662E-01	1.5976	1510.0	.11068E-01
19	.34676E-01	.35698F-01	1.6045	1497.2	.11736E-01
20	.34711E-01	.35735F-01	1.6115	1483.8	.12410E-01
21	.34747E-01	.35772E-01	1.6186	1470.3	.13090E-01
22	.34782E-01	.35809F-01	1.6257	1457.0	.13777E-01
23	.34818E-01	.35845F-01	1.6329	1443.0	.14469E-01
24	.34854E-01	.35882F-01	1.6401	1430.0	.15168E-01
25	.34889E-01	.35919E-01	1.6474	1417.4	.15874E-01
26	.34925E-01	.35956E-01	1.6547	1404.4	.16586E-01
27	.34960E-01	.35992F-01	1.6621	1391.4	.17305E-01
28	.35006E-01	.36029E-01	1.6696	1378.5	.18030E-01
29	.35041E-01	.36066F-01	1.6771	1365.7	.18762E-01
30	.35077E-01	.36103F-01	1.6847	1353.0	.19501E-01
31	.35112E-01	.36139E-01	1.6923	1340.3	.20247E-01
32	.35148E-01	.36176F-01	1.7000	1327.7	.21001E-01
33	.35184E-01	.36213E-01	1.7078	1315.2	.21761E-01
34	.35219E-01	.36250E-01	1.7156	1302.7	.22529E-01
35	.35255E-01	.36287F-01	1.7235	1290.4	.23304E-01
36	.35290E-01	.36323E-01	1.7315	1278.1	.24086E-01
37	.35326E-01	.36360E-01	1.7395	1265.9	.24876E-01
38	.35362E-01	.36397E-01	1.7476	1253.7	.25674E-01
39	.35397E-01	.36433E-01	1.7557	1241.7	.26479E-01
40	.35433E-01	.36470F-01	1.7639	1229.7	.27292E-01
41	.35468E-01	.36507F-01	1.7722	1217.8	.28113E-01
42	.35504E-01	.36544F-01	1.7805	1206.0	.28942E-01
43	.35539E-01	.36580E-01	1.7889	1194.2	.29780E-01
44	.35575E-01	.36617E-01	1.7974	1182.6	.30625E-01
45	.35610E-01	.36654F-01	1.8060	1171.0	.31479E-01
46	.35646E-01	.36691E-01	1.8146	1159.5	.32342E-01
47	.35681E-01	.36728E-01	1.8232	1148.0	.33213E-01
48	.35717E-01	.36764F-01	1.8320	1136.7	.34093E-01
49	.35752E-01	.36801F-01	1.8408	1125.4	.34981E-01
50	.35788E-01	.36838F-01	1.8496	1114.2	.35879E-01
51	.35823E-01	.36875E-01	1.8586	1103.1	.36785E-01
52	.35859E-01	.36911E-01	1.8676	1092.1	.37701E-01
53	.35894E-01	.36948F-01	1.8767	1081.1	.38626E-01
54	.35930E-01	.36985F-01	1.8858	1070.3	.39560E-01
55	.35965E-01	.37022F-01	1.8950	1059.5	.40504E-01
56	.36001E-01	.37058F-01	1.9043	1048.7	.41458E-01
57	.36036E-01	.37095F-01	1.9137	1038.1	.42421E-01
58	.36072E-01	.37132E-01	1.9231	1027.0	.43394E-01
59	.36107E-01	.37169E-01	1.9326	1017.1	.44377E-01
60	.36143E-01	.37205F-01	1.9422	1006.7	.45371E-01
61	.36178E-01	.37242F-01	1.9519	996.36	.46374E-01
62	.36214E-01	.37279F-01	1.9616	986.12	.47388E-01

63	.30941E-01	.37310E-01	1.9714	975.96	.48413E-01
64	.30976E-01	.37352E-01	1.9813	965.88	.49448E-01
65	.30912E-01	.37389E-01	1.9912	955.88	.50495E-01
66	.30747E-01	.37420E-01	2.0012	945.96	.51552E-01
67	.30683E-01	.37463E-01	2.0113	936.12	.52620E-01
68	.30619E-01	.37499E-01	2.0215	926.35	.53699E-01
69	.30554E-01	.37530E-01	2.0318	916.67	.54790E-01
70	.30490E-01	.37573E-01	2.0421	907.06	.55893E-01
71	.30425E-01	.37610E-01	2.0525	897.53	.57007E-01
72	.30361E-01	.37640E-01	2.0630	888.08	.58133E-01
73	.30296E-01	.37683E-01	2.0735	878.70	.59271E-01
74	.30232E-01	.37720E-01	2.0842	869.41	.60421E-01
75	.30168E-01	.37757E-01	2.0949	860.19	.61584E-01
76	.30103E-01	.37793E-01	2.1057	851.05	.62759E-01
77	.30039E-01	.37830E-01	2.1166	841.98	.63946E-01
78	.29974E-01	.37867E-01	2.1275	832.99	.65147E-01
79	.29910E-01	.37904E-01	2.1386	824.08	.66360E-01
80	.29845E-01	.37940E-01	2.1497	815.25	.67587E-01
81	.29781E-01	.37977E-01	2.1609	806.49	.68827E-01
82	.29716E-01	.38014E-01	2.1722	797.81	.70080E-01
83	.29652E-01	.38051E-01	2.1835	789.20	.71348E-01
84	.29588E-01	.38087E-01	2.1950	780.66	.72629E-01
85	.29523E-01	.38124E-01	2.2065	772.21	.73923E-01
86	.29459E-01	.38161E-01	2.2181	763.82	.75233E-01
87	.29394E-01	.38198E-01	2.2298	755.51	.76556E-01
88	.29330E-01	.38234E-01	2.2416	747.28	.77894E-01
89	.29265E-01	.38271E-01	2.2535	739.12	.79247E-01
90	.29201E-01	.38308E-01	2.2655	731.03	.80615E-01
91	.29137E-01	.38345E-01	2.2775	723.02	.81998E-01
92	.29072E-01	.38382E-01	2.2897	715.07	.83397E-01
93	.29008E-01	.38418E-01	2.3019	707.20	.84811E-01
94	.28943E-01	.38455E-01	2.3142	699.41	.86241E-01
95	.28879E-01	.38492E-01	2.3266	691.68	.87686E-01
96	.28814E-01	.38529E-01	2.3391	684.03	.89148E-01
97	.28750E-01	.38565E-01	2.3517	676.44	.90627E-01
98	.28686E-01	.38602E-01	2.3643	668.93	.92122E-01
99	.28621E-01	.38639E-01	2.3771	661.49	.93633E-01
100	.28557E-01	.38676E-01	2.3900	654.11	.95162E-01
101	.28492E-01	.38712E-01	2.4029	646.81	.96708E-01
102	.28428E-01	.38749E-01	2.4159	639.57	.98272E-01
103	.28363E-01	.38786E-01	2.4291	632.41	.99853E-01
104	.28299E-01	.38823E-01	2.4423	625.31	.10145
105	.28235E-01	.38859E-01	2.4556	618.28	.10307
106	.28170E-01	.38896E-01	2.4690	611.32	.10471
107	.28106E-01	.38933E-01	2.4826	604.42	.10636
108	.28041E-01	.38970E-01	2.4962	597.59	.10803
109	.27977E-01	.39006E-01	2.5099	590.83	.10973
110	.27912E-01	.39043E-01	2.5237	584.14	.11144
111	.27848E-01	.39080E-01	2.5376	577.51	.11317
112	.27784E-01	.39117E-01	2.5516	570.94	.11492
113	.27719E-01	.39153E-01	2.5657	564.44	.11669
114	.27655E-01	.39190E-01	2.5799	558.00	.11848
115	.27590E-01	.39227E-01	2.5942	551.63	.12030
116	.27526E-01	.39264E-01	2.6086	545.32	.12213
117	.27461E-01	.39300E-01	2.6231	539.07	.12399
118	.27397E-01	.39337E-01	2.6377	532.89	.12586
119	.27332E-01	.39374E-01	2.6524	526.77	.12776
120	.27268E-01	.39411E-01	2.6672	520.71	.12968
121	.27204E-01	.39447E-01	2.6821	514.71	.13162
122	.27139E-01	.39484E-01	2.6971	508.77	.13359
123	.27075E-01	.39521E-01	2.7123	502.89	.13558
124	.27011E-01	.39558E-01	2.7275	497.07	.13759
125	.26946E-01	.39594E-01	2.7428	491.31	.13963
126	.26881E-01	.39631E-01	2.7583	485.61	.14169
127	.26817E-01	.39668E-01	2.7738	479.97	.14377
128	.26753E-01	.39705E-01	2.7895	474.39	.14588

129	.26688E-01	.39741E-01	2.8052	468.86	.14801
130	.26624E-01	.39778E-01	2.8211	463.39	.15017
131	.26559E-01	.39815E-01	2.8371	457.98	.15235
132	.26495E-01	.39852E-01	2.8532	452.62	.15456
133	.26430E-01	.39888E-01	2.8694	447.32	.15680
134	.26366E-01	.39925E-01	2.8858	442.08	.15906
135	.26302E-01	.39962E-01	2.9022	436.89	.16135
136	.26237E-01	.39999E-01	2.9188	431.76	.16366
137	.26173E-01	.40036E-01	2.9354	426.68	.16601
138	.26108E-01	.40072E-01	2.9522	421.65	.16838
139	.26044E-01	.40109E-01	2.9691	416.68	.17078
140	.25979E-01	.40146E-01	2.9861	411.76	.17321
141	.25915E-01	.40183E-01	3.0033	406.89	.17566
142	.25851E-01	.40219E-01	3.0205	402.07	.17815
143	.25786E-01	.40256E-01	3.0379	397.31	.18067
144	.25722E-01	.40293E-01	3.0554	392.59	.18322
145	.25657E-01	.40330E-01	3.0730	387.93	.18579
146	.25593E-01	.40366E-01	3.0908	383.32	.18840
147	.25528E-01	.40403E-01	3.1086	378.75	.19104
148	.25464E-01	.40440E-01	3.1266	374.24	.19371
149	.25399E-01	.40477E-01	3.1447	369.77	.19642
150	.25335E-01	.40513E-01	3.1630	365.36	.19916
151	.25271E-01	.40550E-01	3.1813	360.99	.20193
152	.25206E-01	.40587E-01	3.1998	356.67	.20473
153	.25142E-01	.40624E-01	3.2184	352.39	.20757
154	.25077E-01	.40660E-01	3.2372	348.16	.21044
155	.25013E-01	.40697E-01	3.2560	343.98	.21335
156	.24948E-01	.40734E-01	3.2751	339.85	.21629
157	.24884E-01	.40771E-01	3.2942	335.76	.21927
158	.24820E-01	.40807E-01	3.3135	331.71	.22228
159	.24755E-01	.40844E-01	3.3329	327.71	.22533
160	.24691E-01	.40881E-01	3.3524	323.76	.22842
161	.24626E-01	.40918E-01	3.3721	319.84	.23155
162	.24562E-01	.40954E-01	3.3919	315.97	.23471
163	.24497E-01	.40991E-01	3.4118	312.15	.23792
164	.24433E-01	.41028E-01	3.4319	308.36	.24116
165	.24368E-01	.41065E-01	3.4521	304.62	.24444
166	.24304E-01	.41101E-01	3.4725	300.92	.24777
167	.24240E-01	.41138E-01	3.4929	297.27	.25113
168	.24175E-01	.41175E-01	3.5136	293.65	.25454
169	.24111E-01	.41212E-01	3.5344	290.07	.25798
170	.24046E-01	.41248E-01	3.5553	286.54	.26147
171	.23982E-01	.41285E-01	3.5764	283.04	.26501
172	.23918E-01	.41322E-01	3.5976	279.58	.26858
173	.23853E-01	.41359E-01	3.6189	276.16	.27220
174	.23789E-01	.41395E-01	3.6404	272.78	.27587
175	.23724E-01	.41432E-01	3.6621	269.44	.27958
176	.23660E-01	.41469E-01	3.6839	266.14	.28334
177	.23595E-01	.41506E-01	3.7058	262.87	.28714
178	.23531E-01	.41542E-01	3.7280	259.64	.29099
179	.23466E-01	.41579E-01	3.7502	256.45	.29489
180	.23402E-01	.41616E-01	3.7726	253.29	.29884
181	.23338E-01	.41653E-01	3.7952	250.17	.30284
182	.23273E-01	.41690E-01	3.8179	247.09	.30689
183	.23209E-01	.41726E-01	3.8408	244.04	.31094
184	.23144E-01	.41763E-01	3.8638	241.02	.31513
185	.23080E-01	.41800E-01	3.8870	238.04	.31933
186	.23015E-01	.41837E-01	3.9104	235.10	.32359
187	.22951E-01	.41873E-01	3.9339	232.19	.32789
188	.22887E-01	.41910E-01	3.9576	229.31	.33226
189	.22822E-01	.41947E-01	3.9815	226.46	.33667
190	.22758E-01	.41984E-01	4.0055	223.65	.34114
191	.22693E-01	.42020E-01	4.0296	220.87	.34567
192	.22629E-01	.42057E-01	4.0540	218.12	.35025
193	.22564E-01	.42094E-01	4.0785	215.40	.35490
194	.22500E-01	.42131E-01	4.1032	212.72	.35960

195	.22434E-01	.42167E-01	4.1281	210.07	.36436
196	.22371E-01	.42204E-01	4.1531	207.44	.36918
197	.22307E-01	.42241E-01	4.1783	204.85	.37406
198	.22242E-01	.42278E-01	4.2037	202.29	.37900
199	.22178E-01	.42314E-01	4.2293	199.75	.38401
200	.22113E-01	.42351E-01	4.2550	197.25	.38908
201	.22048E-01	.42388E-01	4.2809	194.78	.39421
202	.21984E-01	.42425E-01	4.3070	192.33	.39941
203	.21920E-01	.42461E-01	4.3333	189.92	.40468
204	.21856E-01	.42498E-01	4.3598	187.53	.41001
205	.21791E-01	.42535E-01	4.3864	185.17	.41541
206	.21727E-01	.42572E-01	4.4133	182.83	.42088
207	.21662E-01	.42608E-01	4.4403	180.53	.42642
208	.21598E-01	.42645E-01	4.4675	178.25	.43203
209	.21534E-01	.42682E-01	4.4949	176.00	.43771
210	.21469E-01	.42719E-01	4.5226	173.77	.44347
211	.21405E-01	.42755E-01	4.5504	171.57	.44930
212	.21340E-01	.42792E-01	4.5784	169.40	.45520
213	.21276E-01	.42829E-01	4.6065	167.25	.46118
214	.21211E-01	.42866E-01	4.6349	165.13	.46723
215	.21147E-01	.42902E-01	4.6635	163.03	.47337
216	.21082E-01	.42939E-01	4.6923	160.96	.47958
217	.21018E-01	.42976E-01	4.7214	158.91	.48587
218	.20954E-01	.43013E-01	4.7506	156.89	.49225
219	.20889E-01	.43049E-01	4.7800	154.88	.49870
220	.20825E-01	.43086E-01	4.8096	152.91	.50524
221	.20760E-01	.43123E-01	4.8395	150.96	.51187
222	.20696E-01	.43160E-01	4.8695	149.03	.51858
223	.20631E-01	.43196E-01	4.8998	147.12	.52538
224	.20567E-01	.43233E-01	4.9303	145.23	.53226
225	.20503E-01	.43270E-01	4.9610	143.37	.53924
226	.20438E-01	.43307E-01	4.9919	141.53	.54630
227	.20374E-01	.43344E-01	5.0231	139.71	.55346
228	.20309E-01	.43380E-01	5.0544	137.92	.56071
229	.20245E-01	.43417E-01	5.0860	136.14	.56806
230	.20180E-01	.43454E-01	5.1179	134.39	.57550
231	.20116E-01	.43491E-01	5.1499	132.66	.58303
232	.20052E-01	.43527E-01	5.1822	130.94	.59067
233	.19987E-01	.43564E-01	5.2148	129.25	.59841
234	.19923E-01	.43601E-01	5.2475	127.58	.60625
235	.19858E-01	.43638E-01	5.2805	125.93	.61419
236	.19794E-01	.43674E-01	5.3138	124.30	.62223
237	.19729E-01	.43711E-01	5.3473	122.68	.63038
238	.19665E-01	.43748E-01	5.3810	121.09	.63864
239	.19601E-01	.43785E-01	5.4150	119.52	.64701
240	.19536E-01	.43821E-01	5.4492	117.96	.65549
241	.19472E-01	.43858E-01	5.4837	116.42	.66408
242	.19407E-01	.43895E-01	5.5185	114.91	.67278
243	.19343E-01	.43932E-01	5.5535	113.41	.68160
244	.19278E-01	.43968E-01	5.5887	111.92	.69053
245	.19214E-01	.44005E-01	5.6242	110.46	.69959
246	.19149E-01	.44042E-01	5.6600	109.01	.70876
247	.19085E-01	.44079E-01	5.6961	107.58	.71805
248	.19021E-01	.44115E-01	5.7324	106.17	.72747
249	.18956E-01	.44152E-01	5.7690	104.78	.73702
250	.18892E-01	.44189E-01	5.8059	103.40	.74669
251	.18827E-01	.44226E-01	5.8430	102.04	.75649
252	.18763E-01	.44262E-01	5.8804	100.69	.76642
253	.18698E-01	.44299E-01	5.9181	99.369	.77648
254	.18634E-01	.44336E-01	5.9561	98.065	.78668
255	.18570E-01	.44373E-01	5.9944	96.776	.79701
256	.18505E-01	.44409E-01	6.0330	95.503	.80748
257	.18441E-01	.44446E-01	6.0718	94.246	.81809
258	.18376E-01	.44483E-01	6.1110	93.003	.82885
259	.18312E-01	.44520E-01	6.1505	91.776	.83974
260	.18247E-01	.44556E-01	6.1902	90.563	.85078

261	.18183E-01	.44593F-01	6.2303	84.365	.86197
262	.18119E-01	.44630E-01	6.2707	86.181	.87332
263	.18054E-01	.44667F-01	6.3114	87.011	.88481
264	.17990E-01	.44703E-01	6.3524	85.856	.89646
265	.17925E-01	.44740F-01	6.3937	84.714	.90826
266	.17861E-01	.44777E-01	6.4353	83.587	.92022
267	.17796E-01	.44814E-01	6.4773	82.472	.93235
268	.17732E-01	.44850E-01	6.5196	81.372	.94468
269	.17668E-01	.44887F-01	6.5622	80.284	.95709
270	.17603E-01	.44924E-01	6.6052	79.210	.96972
271	.17539E-01	.44961E-01	6.6485	78.149	.98251
272	.17474E-01	.44998F-01	6.6921	77.100	.99548
273	.17410E-01	.45034E-01	6.7361	76.065	1.0086

CYCLES TO FAILURE

CYCLES	USAGE FACTOR
272	.9955
273	1.0086

APPENDIX B

FINITE ELEMENT ANALYSIS

INTRODUCTION

The MARC general purpose finite element computer program was adopted to study the response of the experimental thrust chamber, during its firing tests. Each test consisted of a chilldown cycle and a number of repetitive firing cycles. Finite element heat transfer and structural analyses were performed on the model. In the heat transfer analysis, the temperature distributions vs. time were obtained for a typical chilldown and firing cycle. In the structural analysis, the resultant temperature distributions and the cyclic pressure loads were used to determine the linear and non-linear response of the structure. Optimized selection of the time and load steps was used for the thermal and elastic-plastic analyses.

THERMAL ANALYSIS

1) Model Description

The finite element mesh used in the analysis is shown in Figure B-1. This model was established based on the geometric symmetry planes and loading conditions. It consists of thirty-five elements and 138 nodal points. All elements are the eight-node planar bi-quadratic quadrilateral type (element 41 in MARC element library). Temperature and position (coordinates) within these elements are interpolated from eight sets of nodal values, the four corner nodes and four mid-side nodes. The interpolation function is such that each edge has a parabolic variation along itself.

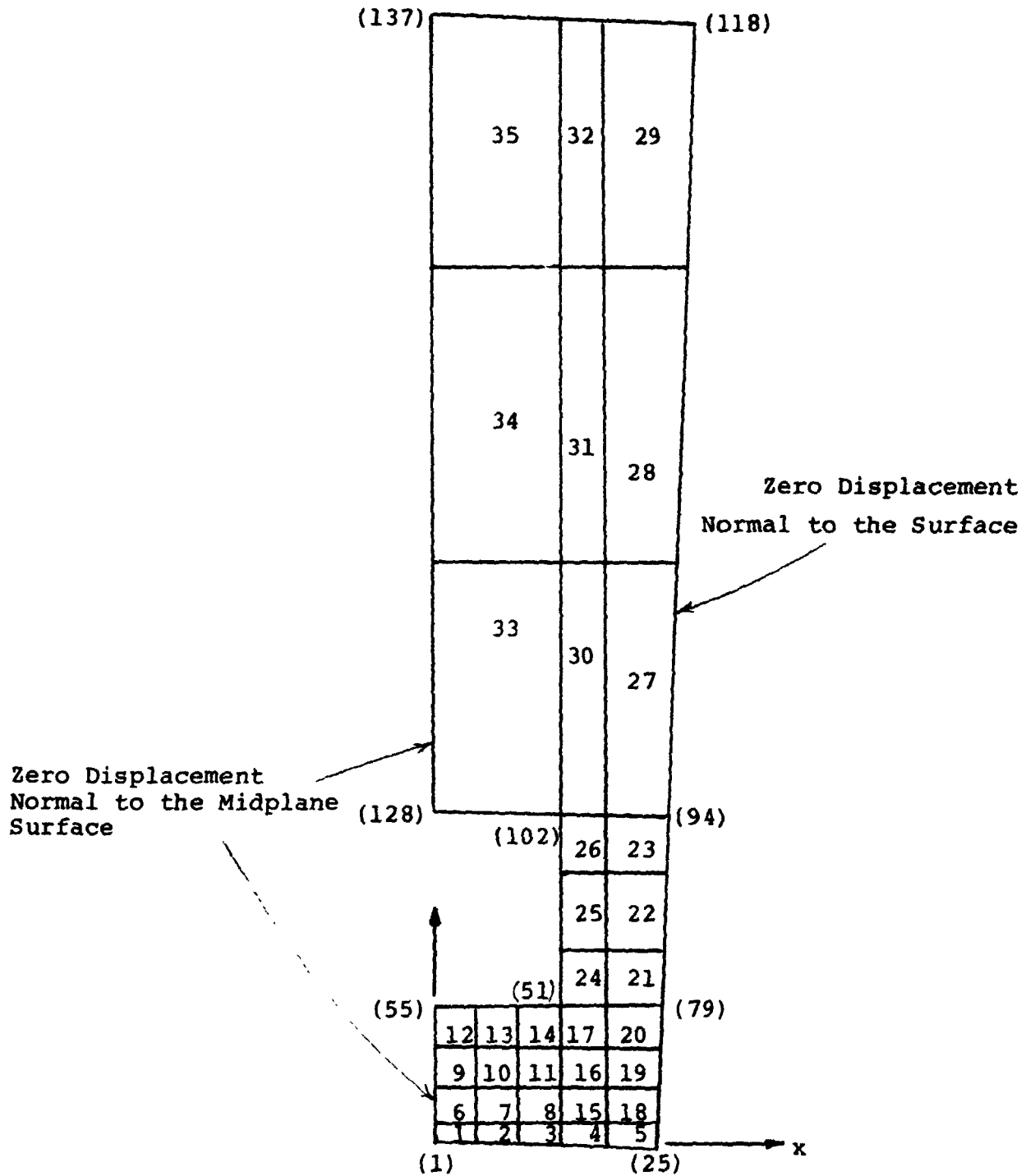


FIGURE B-1 FINITE ELEMENT MODEL OF THE NOZZLE

2) Material Properties

The properties used to characterize the response of the nozzle in the thermal analysis were obtained from Reference 3. They were thermal conductivity and specific heat as a function of temperature of the thrust chamber material as shown in Figures B-2 and B-3, respectively.

3) Load Cycles

The thermal analysis consisted of a chilldown and a firing cycle which lasted 1.5 and 3.5 seconds, respectively. At the beginning of the chilldown period, the room temperature value of 294°K (530°R) was assumed to be the uniform initial temperature of the entire thrust chamber. The thermal operating conditions (heat transfer coefficient) were defined in terms of thermal boundary conditions on the cooling channel surfaces (cold side) and the combustion gas surface (hot side). These boundary conditions for the chilldown and a firing cycle (totally five seconds) are plotted vs. time in Figures B-4a through B-4D. To improve the convergence process, the temperature of the coolant flow at the beginning of the chilldown period was assumed to be the same as the initial model temperature 294°K (530°R), and then it was suddenly dropped to 29°K (53°R) in 0.1 second. For more accuracy in results of the heat transfer analysis, the time steps were controlled by the program to limit the maximum temperature change at any node to 28°K (50°R).

4) Results of Heat Transfer Analysis

The heat transfer analysis of the model was completed in 107 iteration cycles, 25 iteration cycles for the chilldown and 82 iteration cycles for a firing cycle. Results show that the temperature of the entire model drops from

ORIGINAL PAGE IS
OF POOR QUALITY

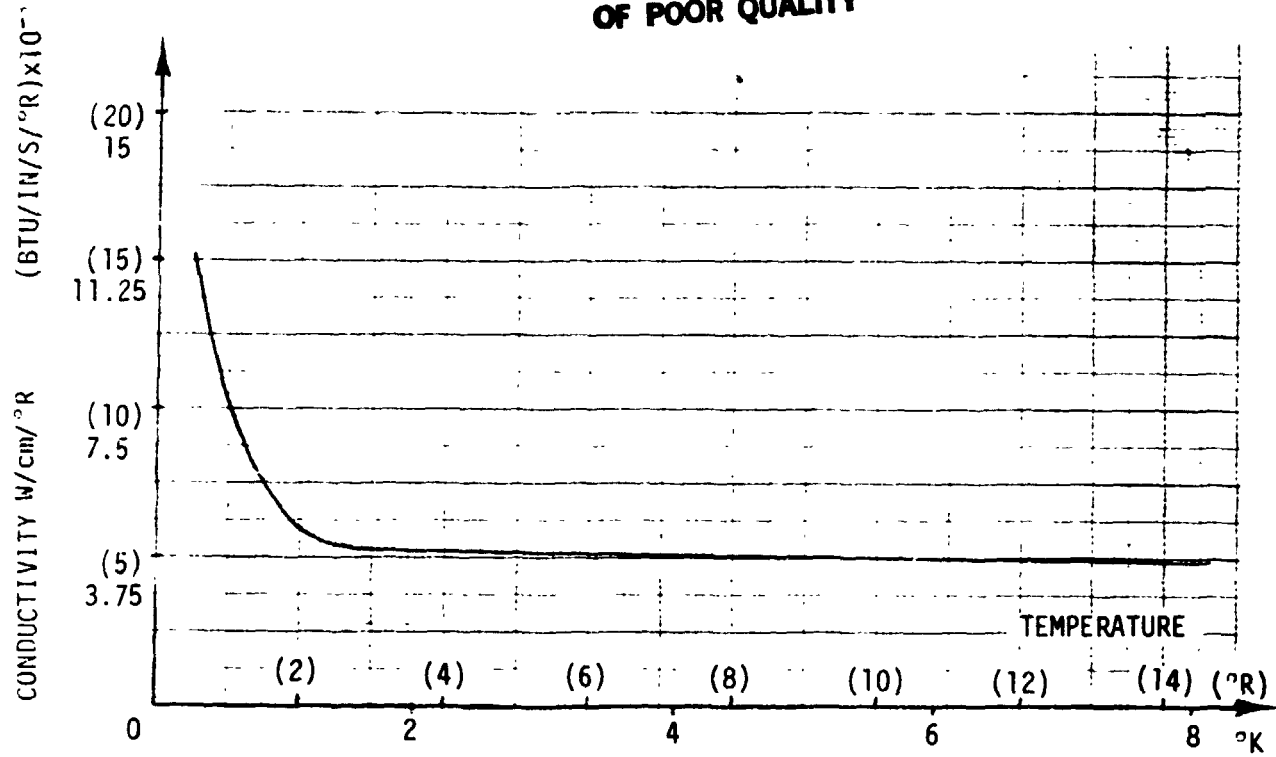


FIGURE B-2 MATERIAL CONDUCTIVITY VS. TEMPERATURE

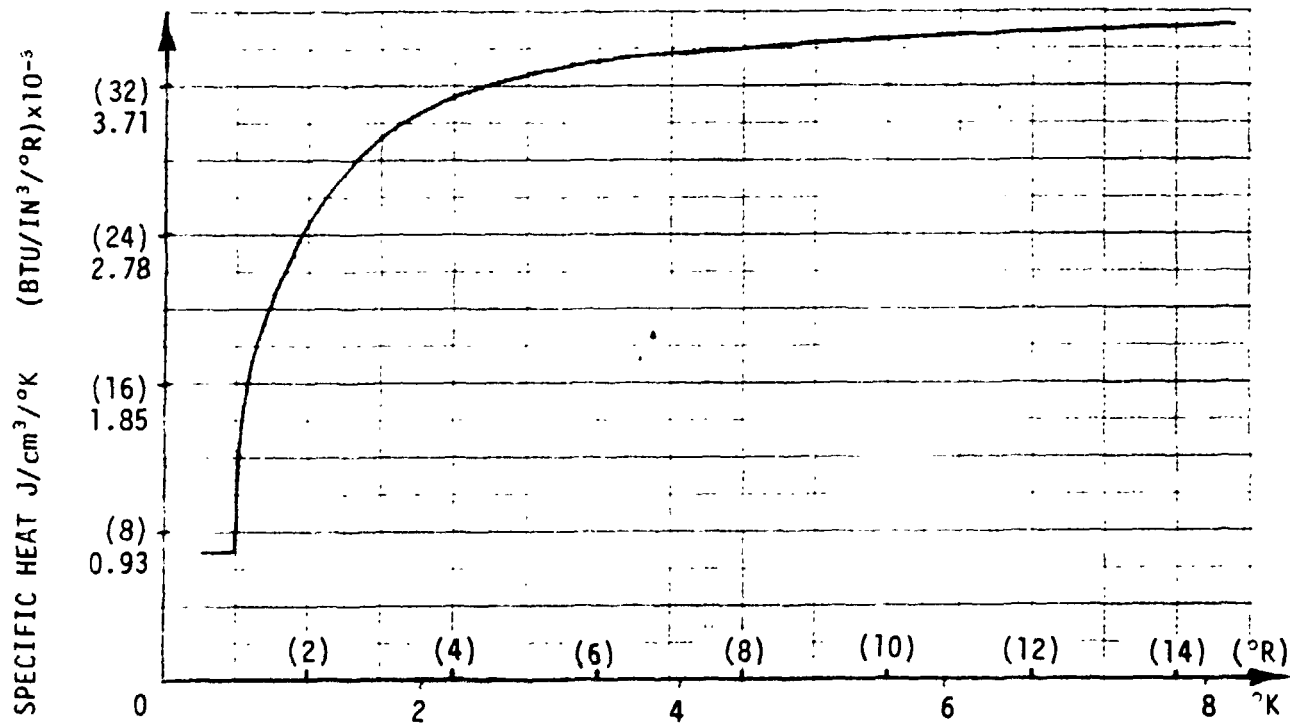


FIGURE B-3 MATERIAL SPECIFIC HEAT VS. TEMPERATURE

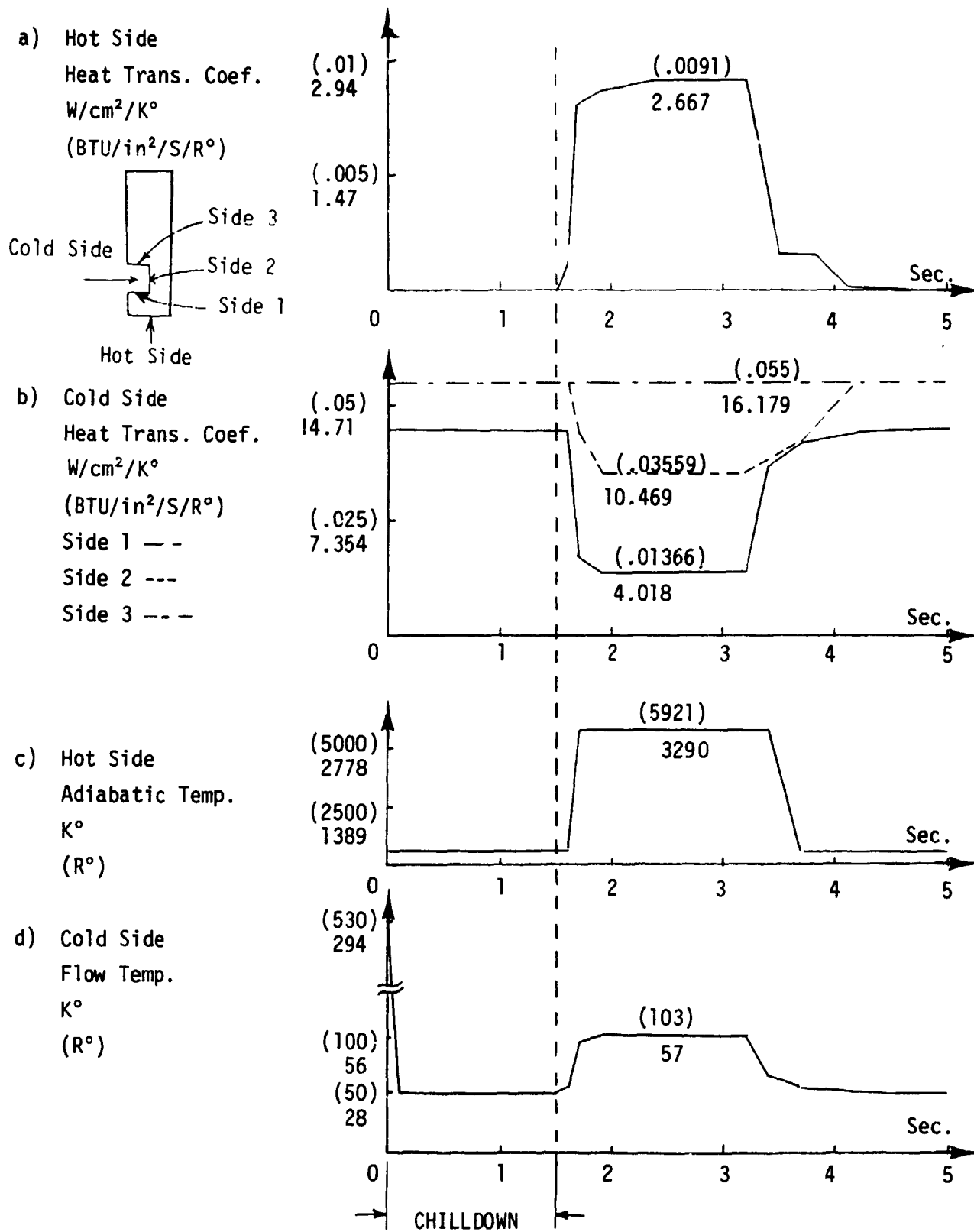


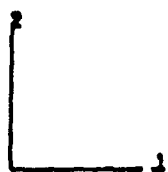
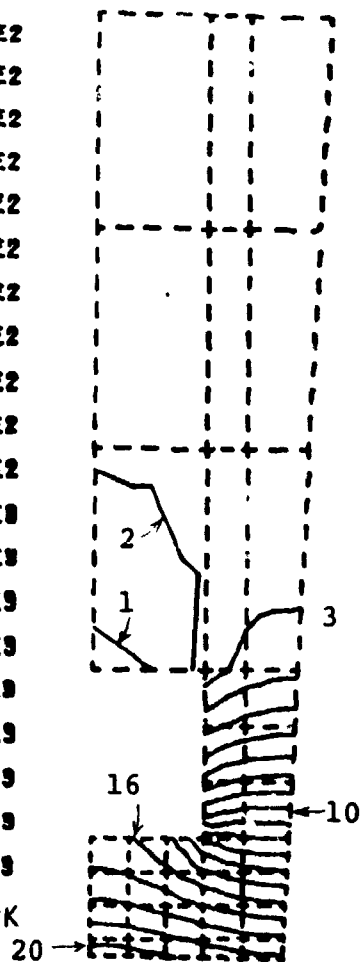
FIGURE B-4 THE TIME HISTORIES OF HEAT TRANSFER COEFFICIENTS AND TEMPERATURES FOR A CHILLDOWN AND FIRING CYCLE

294°K (530°R) at $t = 0$ to less than 30°K (54°R) at $t = 0.65$ second and to a uniform temperature of 29°K (53°R) at $t = 1.13$ seconds. From $t = 1.13$ to $t = 1.5$ seconds the nozzle remains at 294°K (530°R) temperature. From $t = 1.5$ seconds which is the start of the firing cycle, the temperature of the model begins to rise until the temperature of the hot surface reaches 805°K (1450°R) at $t = 3.2$ seconds. At this point the temperature of the model begins to drop until the entire model reaches the temperature of 29°K (53°R) at $t = 5.5$ seconds.

To get a picture of the temperature distribution, plots of continuous isotherms at $t = 3.2$ seconds are reproduced in Figure B-5. The temperature distribution of the centerline of the model is also plotted at different time intervals in a firing cycle in Figure B-6. It appears from the results that the maximum temperature difference between the hot and cold surfaces is 114°K (206°R) and the maximum temperature difference between the hot surface and the outer surface of the model is 225°K (946°R) during the time interval of $t = 1.9$ to $t = 3.2$ sec. The temperature histories of a few selected points are also plotted for a chilldown and firing cycle in Figure B-7. Since the temperature of the entire thrust chamber approached 29°K (53°R) at the end of the first firing cycle, it was concluded that the thermal analysis of this cycle without the chilldown could be used to simulate the remaining cycles.

CURVE NO. (°R)

- 1 = 4 .72E2
 - 2 = 5 .23E2
 - 3 = 6 .73E2
 - 4 = 8 .23E2
 - 5 = 8 .73E2
 - 6 = 7 .23E2
 - 7 = 7 .74E2
 - 8 = 8 .24E2
 - 9 = 8 .74E2
 - 10 = 8 .24E2
 - 11 = 8 .74E2
 - 12 = 1 .02E9
 - 13 = 1 .07E9
 - 14 = 1 .13E9
 - 15 = 1 .18E9
 - 16 = 1 .23E9
 - 17 = 1 .28E9
 - 18 = 1 .33E9
 - 19 = 1 .38E9
 - 20 = 1 .43E9
- 1°R = 0.55°K



TEMP. DIST. RUN 42

FIGURE B-5 ISOTHERM PLOTS AT t=3.2 SECONDS

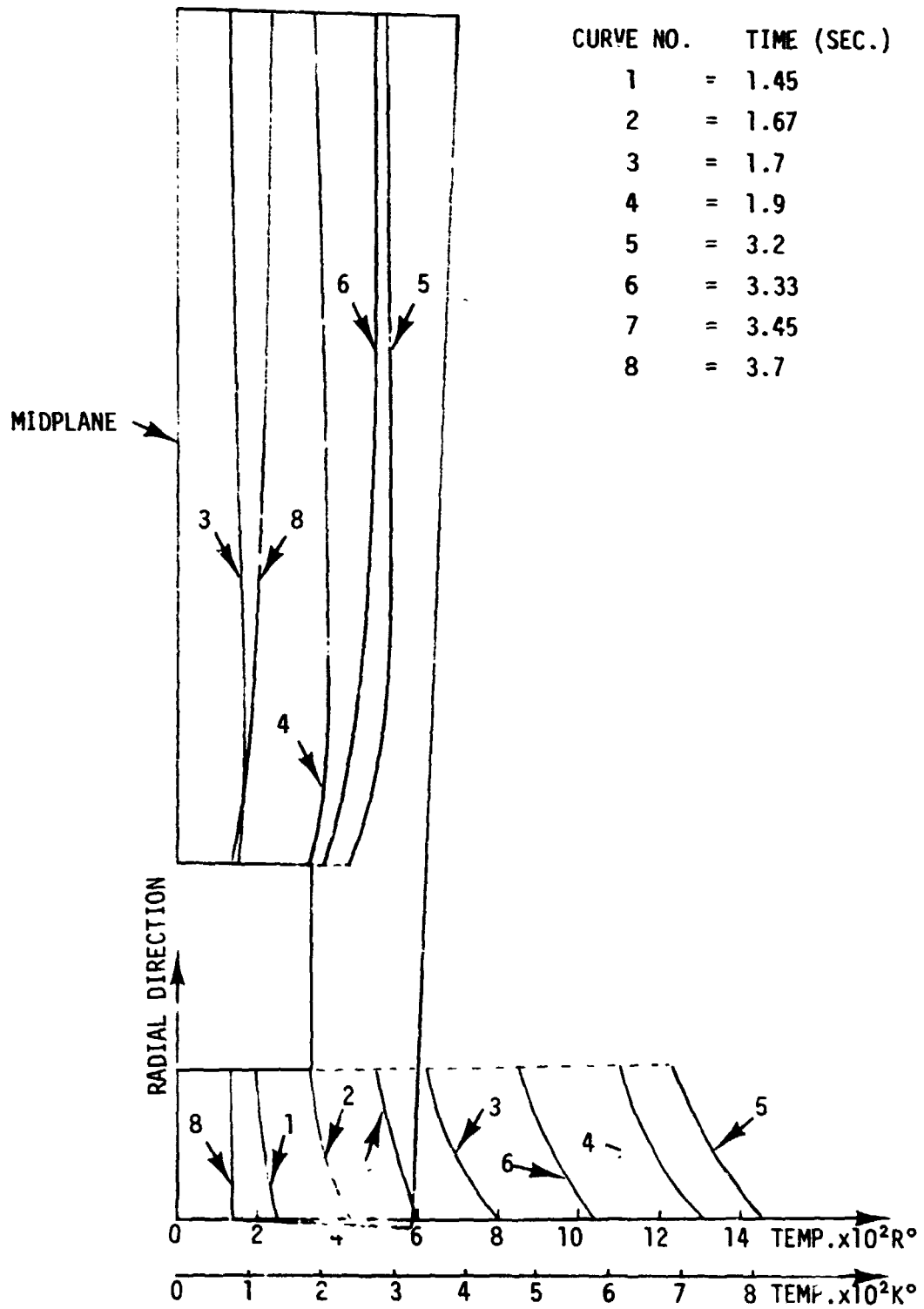


FIGURE B-6 MIDPLANE TEMPERATURE HISTORY

ORIGINAL PAGE IS
OF POOR QUALITY

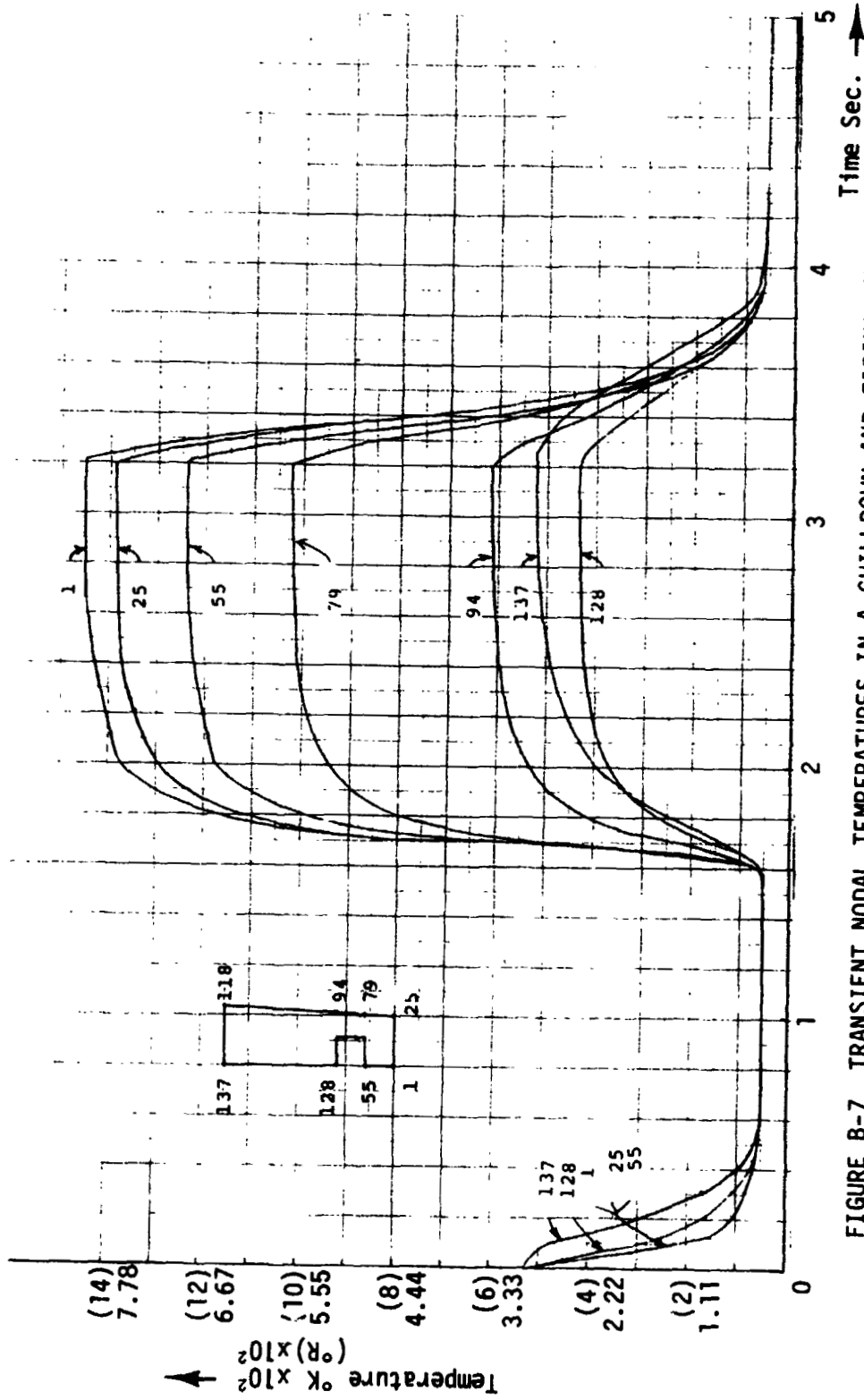


FIGURE B-7 TRANSIENT NODAL TEMPERATURES IN A CHILLDOWN AND FIRING CYCLE

STRUCTURAL ANALYSIS

1) Model Description

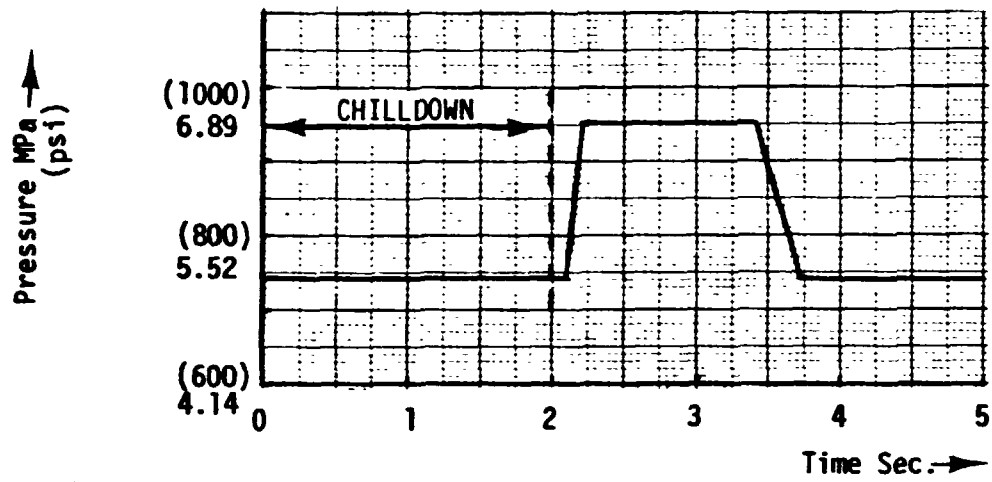
The finite element mesh used in the structural analysis is the same as the one used for heat transfer analysis. Eight-node isoparametric distorted quadrilateral generalized plane strain elements are used for the structural analysis. Displacement and position (coordinates) within the element are interpolated from eight sets of nodal values. The four corners and four mid-side nodes. The interpolation function is such that each edge has parabolic variation along itself.

2) Material Properties

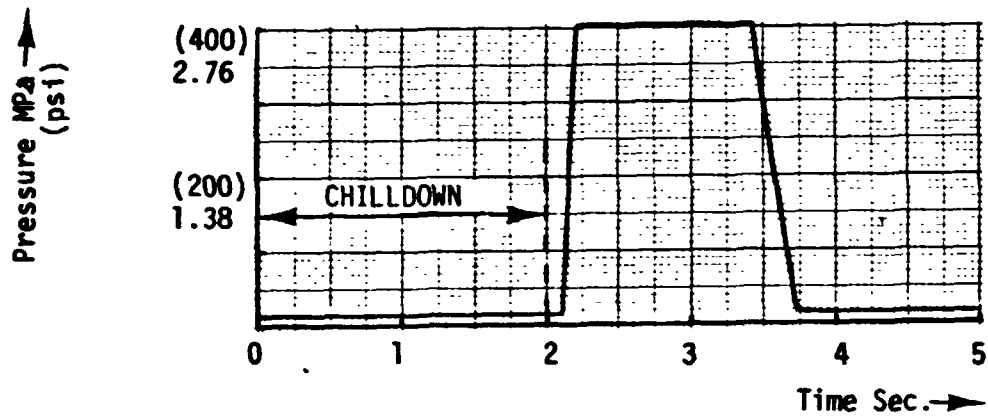
The properties used to characterize the response of the thrust chamber in the structural analysis were taken from Ref. 3. They were time-dependent thermal expansion, Modulus of Elasticity, and stress-strain curves (work hardening).

3) Loading Cycles

The temperature distribution from the heat transfer analysis and the corresponding cyclic pressure load were supplied to the structural analysis program. The cyclic pressure load as a function of time is plotted in Figure B-8. The structural analysis was performed for a chill-down and two consecutive firing cycles. Due to the non-linear response of the thrust chamber material, iteration cycles were controlled to limit the maximum temperature change input to the structural analysis to 13.9°C (25°F) at any node. Both isotropic and kinematic work hardening were used in the analysis.



a) Cold Side Pressure



b) Hot Side Pressure

FIGURE B-8 CYCLIC PRESSURE LOAD VS. TIME

4) Results of Structural Analysis

The structural analysis of the model was completed in thirty-four (34) iteration cycles simulating the chillover and 130 iteration cycles simulating each firing cycle. Some plots of typical stress and strain distributions are reproduced in Figures B-9 through B-14.

CURVE NO.	(psi)
1	= 2 .17E2
2	= 4 .43E2
3	= 6 .68E2
4	= 8 .93E2
5	= 1 .12E3
6	= 1 .34E3
7	= 1 .57E3
8	= 1 .79E3
9	= 2 .02E3
10	= 2 .24E3

1 psi = 6.895 kPa

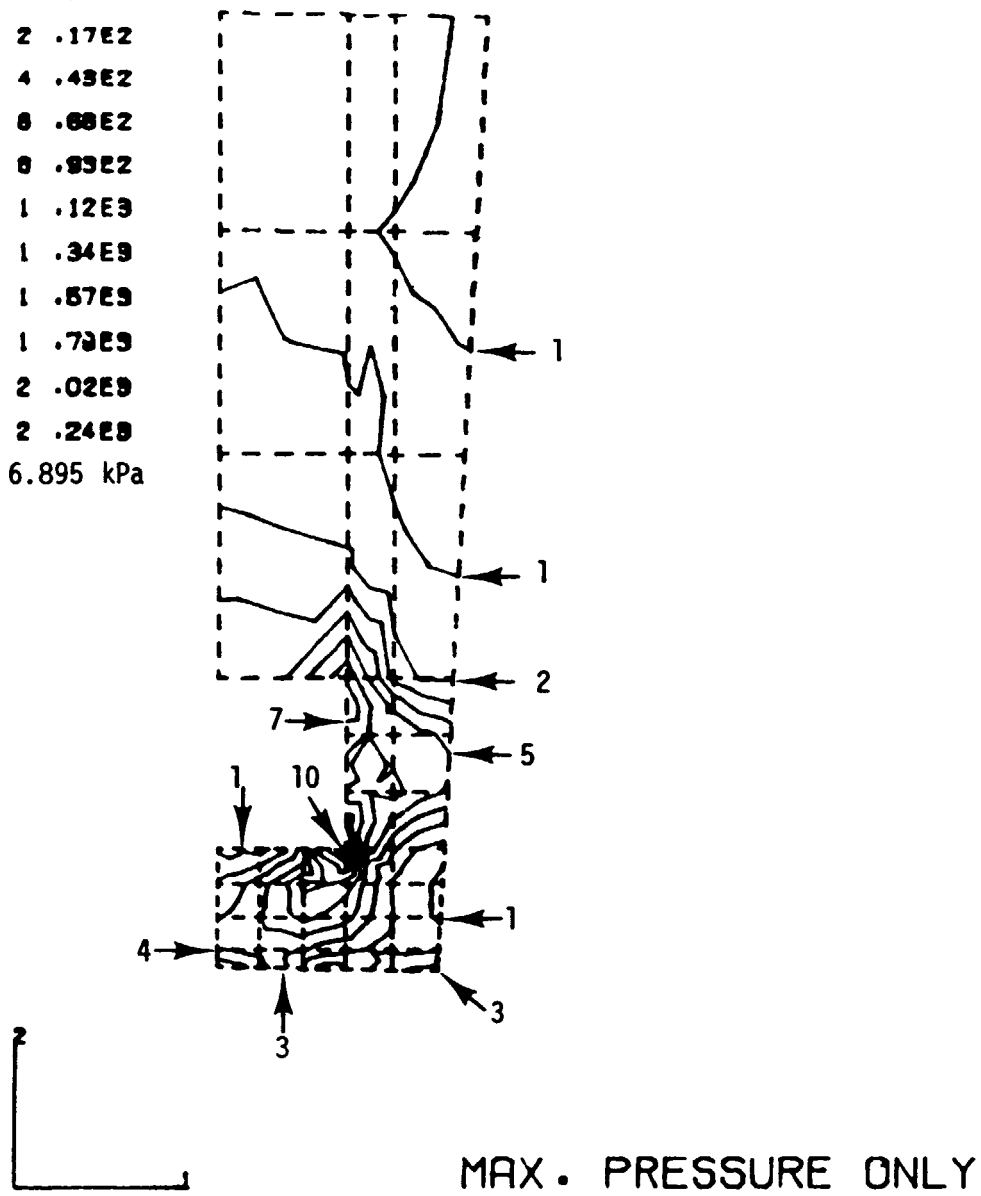


FIGURE B-9 STRESS INTENSITY (VON MISES) DISTRIBUTION FOR THE MAXIMUM PRESSURE DIFFERENCE (ELASTIC ANALYSIS)

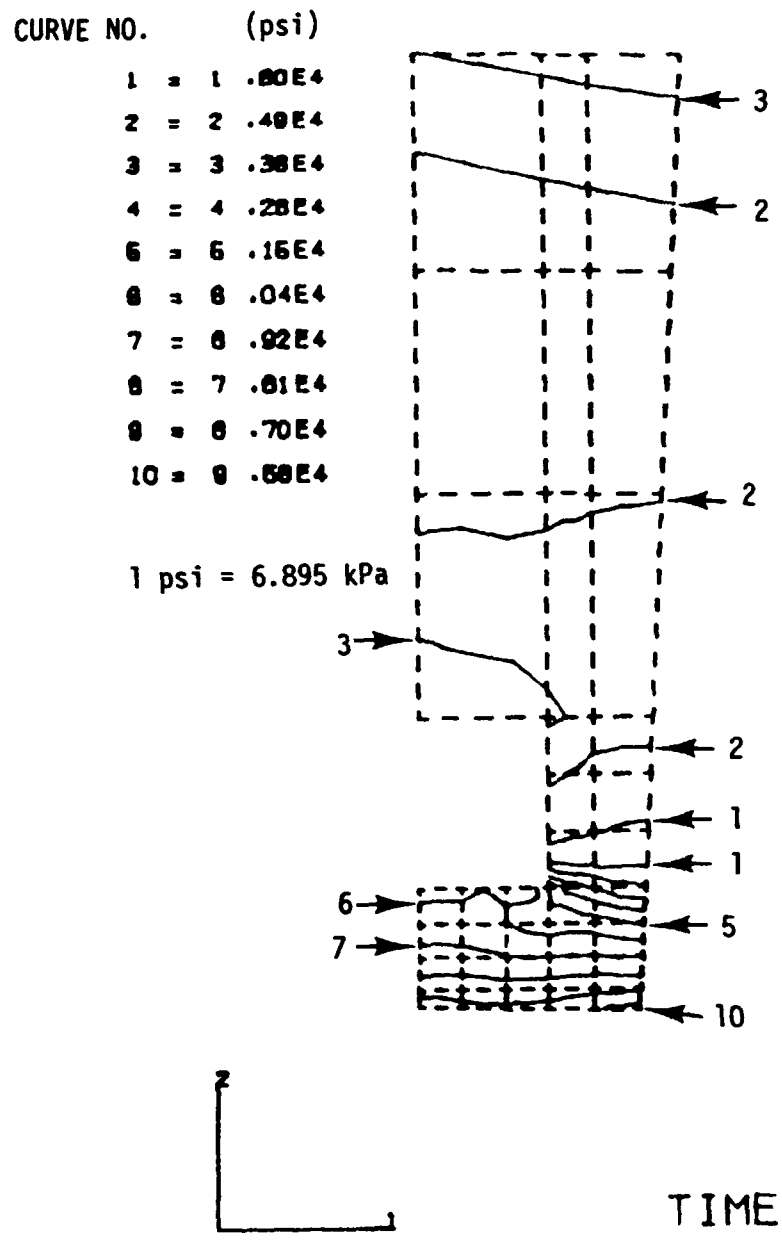
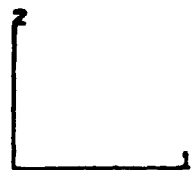
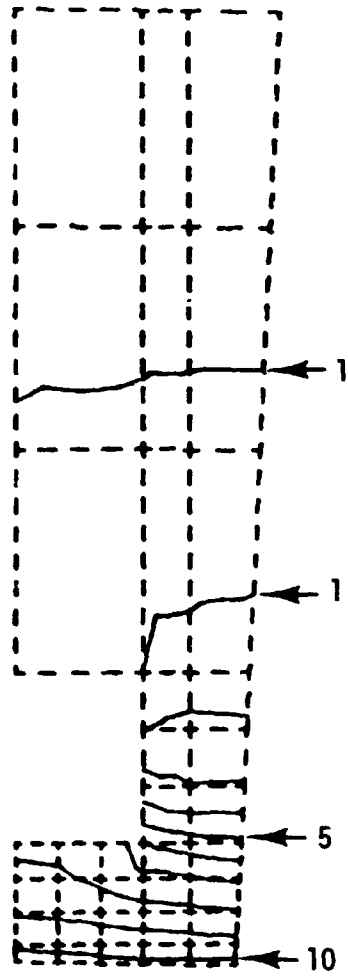


FIGURE B-10 STRESS INTENSITY (VON MISES) DISTRIBUTION AT TIME = 0.2 SECONDS AFTER THE BEGINNING OF THE FIRST FIRING CYCLE (ELASTIC ANALYSIS)

CURVE NO.

- 1 = $-4.48E-3$
- 2 = $-3.38E-3$
- 3 = $-2.28E-3$
- 4 = $-1.17E-3$
- 5 = $-8.88E-5$
- 6 = $1.04E-3$
- 7 = $2.14E-3$
- 8 = $3.25E-3$
- 9 = $4.35E-3$
- 10 = $5.45E-3$



TIME=1.7

FIGURE B-11 STRAIN DISTRIBUTION IN THE RADIAL DIRECTION AT TIME = 0.2 SECONDS AFTER THE BEGINNING OF THE FIRST FIRING CYCLE (ELASTIC ANALYSIS)

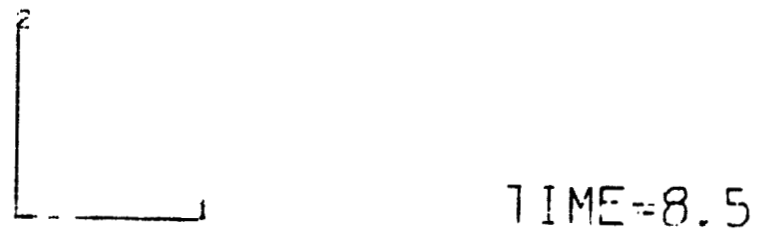
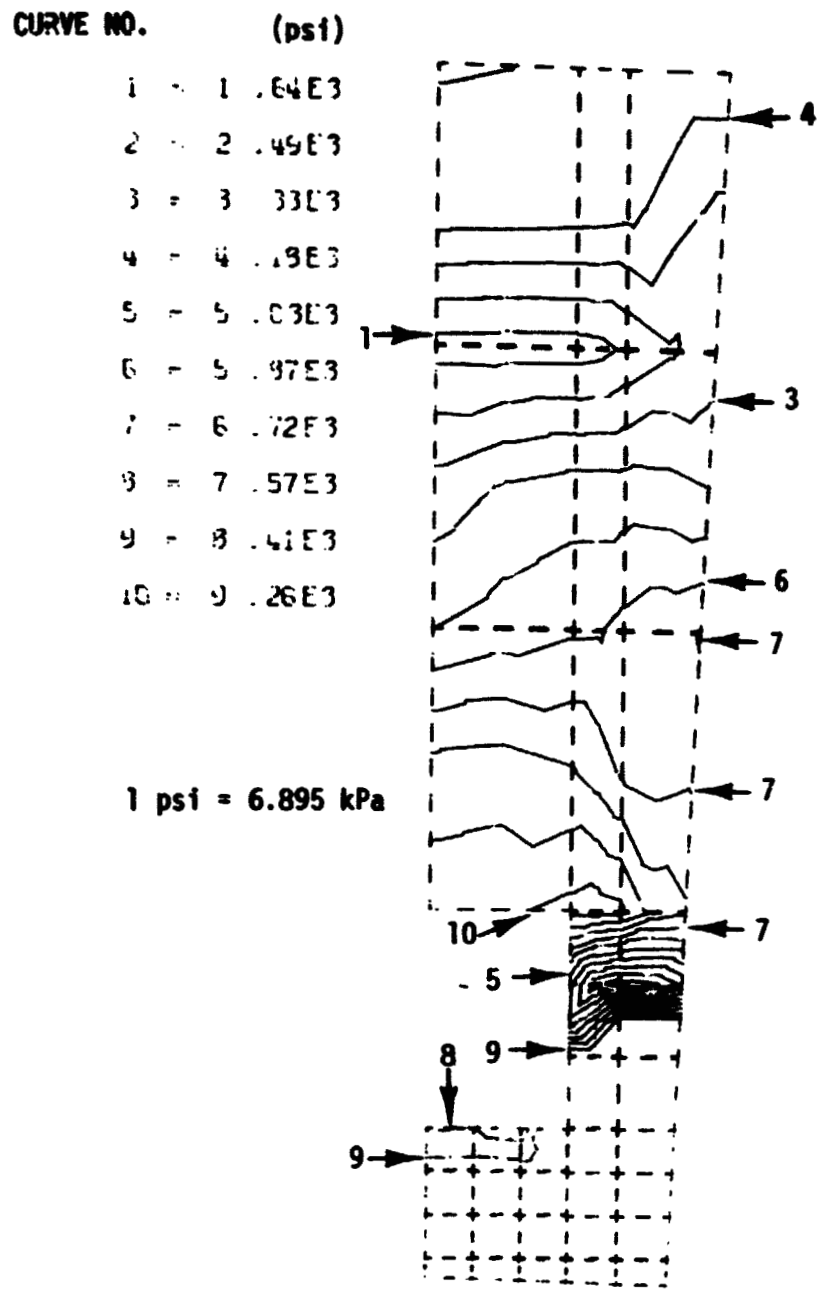


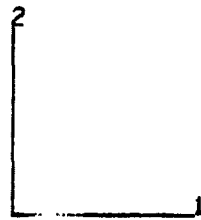
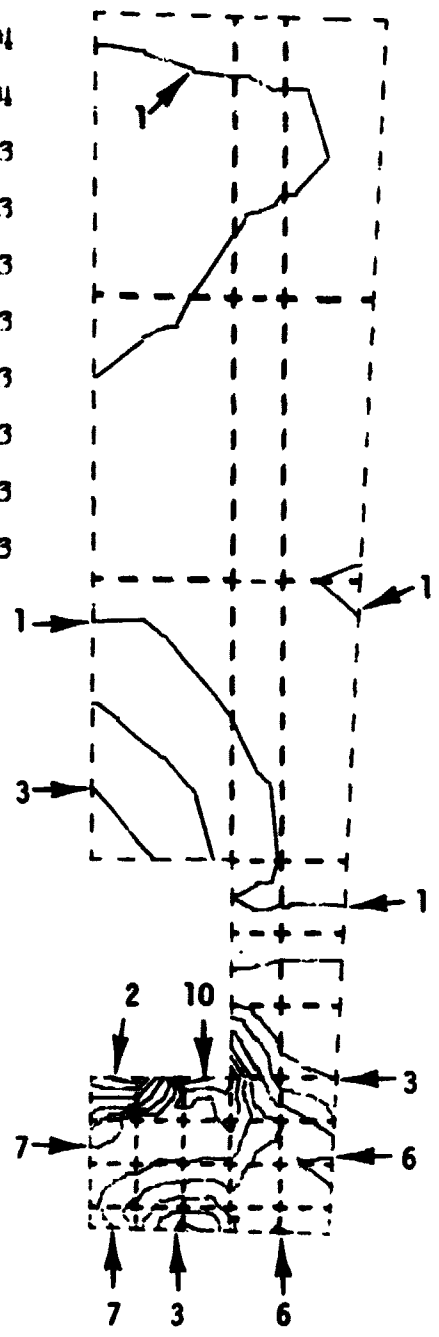
FIGURE B-12 STRESS INTENSITY (VON MISES) DISTRIBUTION AT THE END OF THE SECOND FIRING CYCLE

ORIGINAL PAGE IS OF POOR QUALITY.

ORIGINAL PAGE IS
OF POOR QUALITY

CURVE NO.

- 1 = 2 .10E-4
- 2 = 7 .68E-4
- 3 = 1 .33E-3
- 4 = 1 .33E-3
- 5 = 2 .44E-3
- 6 = 3 .00E-3
- 7 = 3 .56E-3
- 8 = 4 .12E-3
- 9 = 4 .67E-3
- 10 = 5 .23E-3



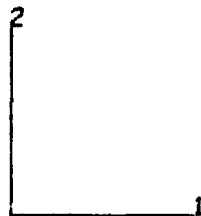
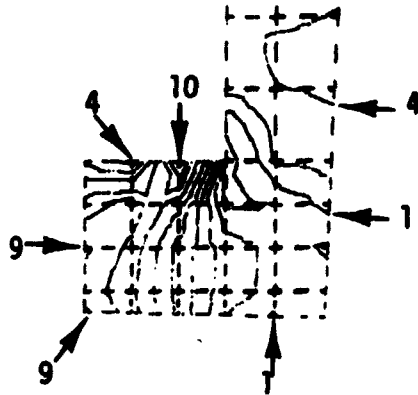
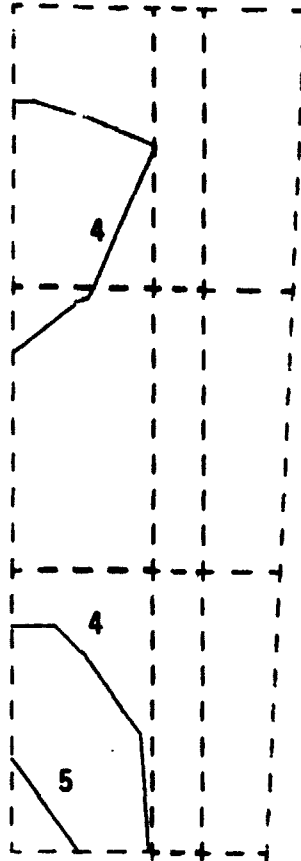
TIME=8.5

FIGURE B-13 TOTAL EQUIVALENT PLASTIC STRAIN DISTRIBUTION AT THE END OF THE SECOND FIRING CYCLE

ORIGINAL PAGE IS
OF POOR QUALITY

CURVE NO.

- 1 - $-1.95E-3$
- 2 - $-1.22E-3$
- 3 - $-4.09E-4$
- 4 - $2.41E-4$
- 5 - $9.72E-4$
- 6 - $1.70E-3$
- 7 - $2.43E-3$
- 8 - $3.16E-3$
- 9 - $3.09E-3$
- 10 - $4.63E-3$



TIME=8.5

FIGURE B-14 PLASTIC STRAIN DISTRIBUTION IN HOOP DIRECTION
AT THE END OF THE SECOND FIRING CYCLE

APPENDIX C

**FORTRAN Program
for
Fatigue Calculation**

ORIGINAL PAGE IS
OF POOR QUALITY

PROGRAM CYCLES 76/76 OPT=1 FTM 4,0+452

```

1      PROGRAM CYCLES(INPUT,OUTPUT)
      REAL N,NF,L
      DIMENSION CYCLE(100),STRAIN(100)
C
C      N= EXPONENT IN STRESS-STRAIN LAW.
C      DELTA= DEFORMATION PER CYCLE
C      E1AVG= AVFRAGE HOOP STRAIN
C      M= HALF THE HEIGHT OF LIGAMENT
C      L= LENGTH OF LIGAMENT
10     C      W= WIDTH OF RIG
C
C      THE FORMAT FOR READING THESE CONSTANTS IS 6F10
C
      READ 200, N,DELTA,E1AVG,M,L,W
C
C      INPUT FATIGUE CURVE
C      NPTS=NUMBER OF DATA POINTS ON FATIGUE CURVE TO BE INPUT
C      MAXIMUM OF 100 POINTS THE FORMAT IS I10
C      CYCLE=CYCLES FOR EACH DATA PT (6F10) RPT CARD IF NPTS,GT,8
C      STRAIN=STRAIN RANGE FOR EACH PT (6F10) RPT CARD IF NPTS,GT,8
20     C
      READ 100, NPTS
      READ 200, (CYCLE(I),I=1,NPTS)
      READ 200, (STRAIN(I),I=1,NPTS)
      PRINT 500, N,DELTA,E1AVG,M,L,W
      DO 5 I=1,NPTS
25     C      5 PRINT 600, CYCLE(I),STRAIN(I)
C
C      CALCULATE CYCLES TO FAILURE
C
30     C      PRINT 700
      USEAGE=0.0
      NCYC=0
      C=(N-1)/N
10     C      NCYC=NCYC+1
35     C      TMIN=(2*M*(L+W)-NCYC*DELTA*M)/(L+W)
      TMAX=(2*M*(L+W)+2*NCYC*DELTA*M)/(L+W)+2
      T=(2*M*(L+W)+2*NCYC*DELTA*M)/(L+W)+(2*M*(L+W)-NCYC*DELTA*M)
      E1MIN=E1AVG*C*(T-1)/(T+C-1)
      E1=E1MIN
      E2=E1AVG
      EEGVT=SQRT((E1-E2)**2+(2*E1+E2)**2+(2*E2+E1)**2)*SQRT(2.)/3
      DO 20 I=2,NPTS
      IF(EEGVT.LE,STRAIN(I-1) .AND. F*EVT.GE,STRAIN(I)) GOTO 30
45     C      20 CONTINUE
      PRINT 300, EEGVT,NCYC
      PRINT 300, USEAGE
      STOP
50     C      30 NF=EXP(ALOG(EEGVT/STRAIN(I-1))/ALOG(STRAIN(I)/STRAIN(I-1)))
      2ALOG(CYCLE(I)/CYCLE(I-1))+ALOG(CYCLE(I-1))
      USEAGE=USEAGE+1./NF
      PRINT 800,NCYC,TMIN,TMAX,EEGVT,NF,USEAGE
      IF(USEAGE.LT.1.0) GO TO 10
C
C      RESULTS
55     C
      PRINT 400, NCYC-1,USEAGE-1./NF,NCYC,USEAGE
      STOP

```

PROGRAM CYCLES 76/76 OPT=1 FTM 4,0+452

```

100  FORMAT(I10)
200  FORMAT(6F10,0)
60   300  FORMAT(1H0,'THE STRAIN RANGE OF ',G12.5,' FOR THE ',I8,' CYCLE IS
      1  NOT ON THE FATIGUE CURVE SUPPLIED')
350  FORMAT(1H0,'THE USAGE FACTOR IS ',F6.4)
400  FORMAT(1H //12X,'CYCLES TO FAILURE',//11X,'CYCLES=',N1,
65   1'USAGE FACTOR',//9X,I8,7X,F6.4//9X,I8,7X,F6.4)
500  FORMAT(1H1,12X,'CONSTANTS INPUT',//11X,' N= ',G12.5//11X,
      2'DELTA= ',G12.5//11X,' E1AVG= ',G12.5//11X,' M= ',G12.5//11X,
      3' L= ',G12.5//11X,' W= ',G12.5//10X,' FATIGUE CURVE',//14X,
      4'CYCLES=',7X,'STRAIN RANGE=')
70   600  FORMAT(1H ,0X,2(4X,G12.5))
      700  FORMAT(1H1,'RESULTS FOR EACH CYCLE IN CYC,TMIN,TMAX,EEGVT,NF,USAGE=
      2/')
800  FORMAT(1H ,5X,I5,5(5X,G12.5))
      END

```

APPENDIX D

SYMBOLS

a	-	axial length
A	-	surface area, also equation arbitrary positive scalar
D	-	rate of dissipation
E	-	modulus of elasticity
E_{el}	-	elastic energy
E_{pl}	-	plastic work
F	-	yield surface
h	-	convective heat transfer coefficient
2H	-	thickness of ligament
k	-	$\sqrt{1-s^2}$; also thermal conductivity
K	-	curvature
l	-	width of ligament in hoop direction
m	-	generalized bending stress variable
M	-	bending moment in ligament
M_o	-	yield bending moment
n	-	generalized hoop stress variable; also strain hardening exponent in stress strain law
N	-	hoop force in ligament; also number of cycles
N_o	-	yield hoop force
p	-	pressure
s	-	generalized shear stress variable
S	-	shear force in ligament

SYMBOLS - continued

S_o	-	yield shear stress
S_y	-	average yield stress in tension
S_{ymin}	-	ligament yield strength for minimum $\alpha(T_i - T_o)$
S_{ymax}	-	ligament yield strength for maximum $\alpha(T_i - T_o)$
t	-	ligament thickness
t_N	-	thinning after N cycles
t_{max}	-	maximum ligament thickness
t_{min}	-	minimum ligament thickness
T	-	temperature
T_i	-	average temperature of ligament
T_o	-	average temperature of closeout wall
w	-	width of rib
z	-	$\bar{\epsilon}/n$, subtangent in Figure 10
α	-	coefficient of thermal expansion; also stress ratio σ_2/σ_1
γ	-	shear strain
δ	-	deflection per cycle
δ_1	-	deflection due to moment
δ_2	-	deflection due to shear
Δp	-	pressure difference between coolant pressure and combustion gas pressure
$\Delta \epsilon_1$	-	total strain range in hoop direction
$\Delta \epsilon_{p_1}$	-	plastic strain range in hoop direction

SYMBOLS - continued

$\Delta \epsilon'_{P1}$	-	plastic strain range in hoop direction due to differential thermal expansion
$\Delta \epsilon''_{P1}$	-	correction to plastic strain range in hoop direction due to thermally induced bending
ϵ	-	hoop strain
ϵ_1	-	hoop strain
ϵ_2	-	axial strain
ϵ_3	-	radial strain
$\epsilon_{1\text{avg}}$	-	average hoop strain in ligament
$\epsilon_{1\text{min}}$	-	hoop strain in minimum ligament section
$\epsilon_{2\text{min}}$	-	axial strain in minimum ligament section
$\epsilon_{3\text{min}}$	-	radial strain in minimum ligament section
$\bar{\epsilon}$	-	effective strain
$\bar{\epsilon}_{\text{cr}}$	-	critical effective strain
$\bar{\epsilon}_{\text{min}}$	-	effective strain in minimum ligament section
ϵ	-	generalized bending strain variable
λ	-	generalized hoop strain variable
ν	-	Poisson's ratio
σ_1	-	hoop stress
σ_2	-	axial stress
σ_b	-	bending stress
$\bar{\sigma}$	-	effective stress
ϕ	-	generalized shear strain variable
.	-	dot above symbol denotes rate